6

MACROMOLECULAR DECORATION OF NANOPARTICLES FOR GUIDING SELF-ASSEMBLY IN 2D AND 3D

Christian Kuttner, Munish Chanana, Matthias Karg, and Andreas Fery

Leibniz-Institut für Polymerforschung Dresden e.V., Institute of Physical Chemistry and Polymer Physics, Germany; Technische Universität Dresden, Physical Chemistry of Polymeric Materials and Cluster of Excellence Centre for Advancing Electronics Dresden (cfaed), Germany; University of Bayreuth, Physical Chemistry I and Physical Chemistry II, Germany; Heinrich Heine University Düsseldorf, Physical Chemistry I, Germany; ETH Zürich, Institute of Building Materials, Switzerland

6.1 INTRODUCTION

Modern functional materials aim at combining different compounds in order to exploit *synergistic effects* or even trigger the *emergence of novel properties*, which neither of the compounds in pure form possesses. Typically, this requires hierarchical organization of nano-/microscale building blocks along the lines of rational design concepts, rather than simple blending of compounds. In fact, in many ways, artificial functional materials approach biological systems, though still far from their complexity [1–3]. Typical examples of such *materials by design* are optical or mechanical metamaterials [4–7], but also modern photovoltaic [8, 9] and optoelectronic devices [10], and nanocomposites [11–15].

In this context, macromolecules play a key role in different perspectives: First, they cover a broad range of length scales between a few nanometers up to several hundred nanometers. As illustrated in Figure 6.1, the critical distances for several important

Macromolecular Self-Assembly, First Edition. Edited by Laurent Billon and Oleg Borisov.

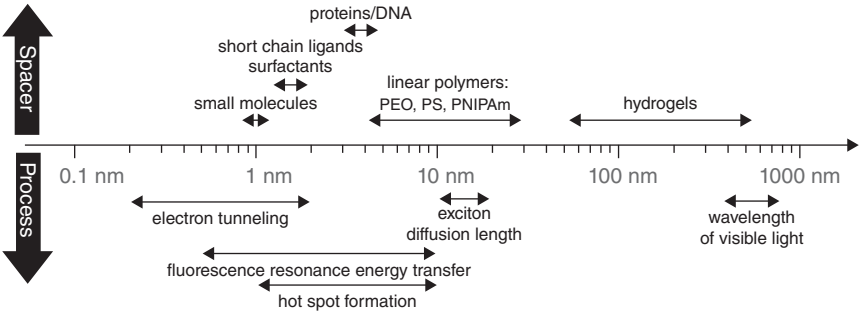

Figure 6.1 Schematic overview showing the correlation of different spacer sizes and physical processes covering the length scales from 0.1 to 1000 nm.

optical and electronic processes fall within this regime. Second, they offer a rich variety of ways for controlling mesostructure formation, for example, as microphase separation for block-copolymer systems [16] or stimuli-responsive assemblies (fibers) for structural protein systems [17–21]. Finally, polymers can be sensitive to a broad range of stimuli such as solvent quality, temperature, pH, salt-concentration, and redox potential [22–25].

In this chapter, we focus on decorating nanoparticles with synthetic as well as biomacromolecules for controlling interparticle distances and relative orientations in assemblies. We introduce synthetic approaches toward core/shell architectures and show how macromolecular ligands allow controlling order in 2D and 3D assemblies. We also illustrate how symmetries can be broken in order to advance from simple hexagonally close-packed assemblies to systems of higher complexity. We put special emphasis on core/gel-shell nanoparticles as a versatile class allowing for large interparticle separations and on protein-modified nanoparticles that are particularly well suited for achieving complex symmetries in particle assemblies. Finally, we point out several examples for functionality, not with the aim of completely covering a specific field of applications but rather for the sake of illustrating the underlying concepts for *functional material design*.

6.2 GUIDING ASSEMBLY BY DECORATION WITH ARTIFICIAL MACROMOLECULES

The state-of-the-art synthesis routes for macromolecular building blocks provide us with excellent structural and compositional control. Parameters relevant for guiding assembly such as molecular weight, wettability/solvent compatibility, steric properties, and conformation can be controlled to a large degree. In this section, we will introduce an overview over the different strategies for coupling macromolecules to nanoparticles in a well-defined fashion, covering both crosslinked and non-crosslinked polymeric coatings. In the following, we will illustrate, how these

coatings can be employed for controlling assembly in two and three dimensions, starting from hexagonal structures up to linear assemblies.

6.2.1 Decoration of Nanoparticles

Nearly all types of nanoparticles feature an organic low-molecular-weight ligand shell, which is inevitable for their synthesis and ensures colloidal stability. The most prominent stabilizers comprise citrate, fatty acids, and other surfactant molecules. Usually these stabilizing molecules are present in huge excess in the as-prepared nanoparticle dispersions. For assembly purposes, this excess concentration has to be reduced by purification procedures such as centrifugation/redispersion, precipitation/redispersion, dialysis, and filtration. Due to the low molecular weight of these stabilizers, only short interparticle distances are achievable in assemblies of the respective nanoparticles. Therefore, for better interparticle distance control, the original stabilizing agents have to be replaced by macromolecules. By controlling the polymer size and architecture, interparticle distances in 2D and 3D assemblies can be finely tuned (Figure 6.1).

The main challenge in decorating nanoparticles with polymers is to anchor the polymer onto the nanoparticle surface. Depending on the surface chemistry of the nanoparticles, different anchoring groups can be employed to attach the polymer robustly onto the nanoparticle surface. In order to remove the initial low-molecular-weight ligand from the surface and bind polymers strongly to the particle surface, these anchoring groups are required to exhibit a larger binding affinity toward the particle surface (large binding constant K) [26]. In general, for metal nanoparticles such as gold or silver nanoparticles, sulfurous groups such as thiols, disulfides, and amine groups are commonly used as anchor groups [27]. For metal oxide nanoparticles, carboxylates, phosphonates, and catechol groups can be employed for attaching polymers to the particle surface [28]. In particular, catechol groups show a high binding affinity toward iron oxide surfaces, even in aqueous dispersion [29–31]. For silica particles, silane chemistry offers a vast library of molecules such as mono-, di-, and trialkoxy or halogenated silanes, thus enabling many different synthetic procedures to anchor organic macromolecules very robustly onto the silica surfaces [32–34]. For organic particles and surfaces, organic coupling reactions can be employed to covalently couple macromolecules on them. Some prominent examples are amide bond coupling (carboxylate + amine), thiol-ene coupling reaction (thiol + unsaturated species) [35, 36], urea-reaction (iso(thio)cyanate + amine), acetal and hemiacetal reactions (ketone or aldehyde + alcohol), imine reaction (ketone or aldehyde + amine), and other click-chemistry approaches (e.g., azide + alkyne) [37–41].

Also multiple anchoring groups, as present in diblock copolymers, yield a robust and permanent attachment of the desired polymer to the particle surface. For more detailed information, the reader is referred to the reviews cited here [42, 43]. Once the right anchoring group has been identified, the polymer chemistry offers many synthetic strategies to functionalize nanoparticles with polymers [41]. With the aid

of various living polymerization techniques developed thus far, a plethora of polymers can be anchored on various types of nanoparticles.

Figure 6.2 gives a schematic representation of available pathways to decorate nanoparticles with macromolecules. Depending on the strategy, different architectures and thicknesses of the polymer layer can be realized. Thus complex polymer coronas have been achieved, such as brush-like architectures with end-tethered chains or gel-like structures with a crosslinked polymer matrix surrounding the nanoparticle cores. The major strategies for the polymer decoration of particles are direct polymer ligand exchange, surface-initiated polymer grafting, and gel-encapsulation upon crosslinking, which will be discussed below in detail.

The first strategy involves the anchoring of pre-synthesized polymer chains (1), which bear specific anchoring/coordination groups for the nanoparticle (see Figure 6.2). When the anchoring group is presented on a terminal position of a polymer chain, the polymer can be tethered onto nanoparticles with one end, yielding brush-type polymer architectures [42]. Hence, this *grafting-onto* technique starts with the design and synthesis of polymeric ligands, with only one terminal

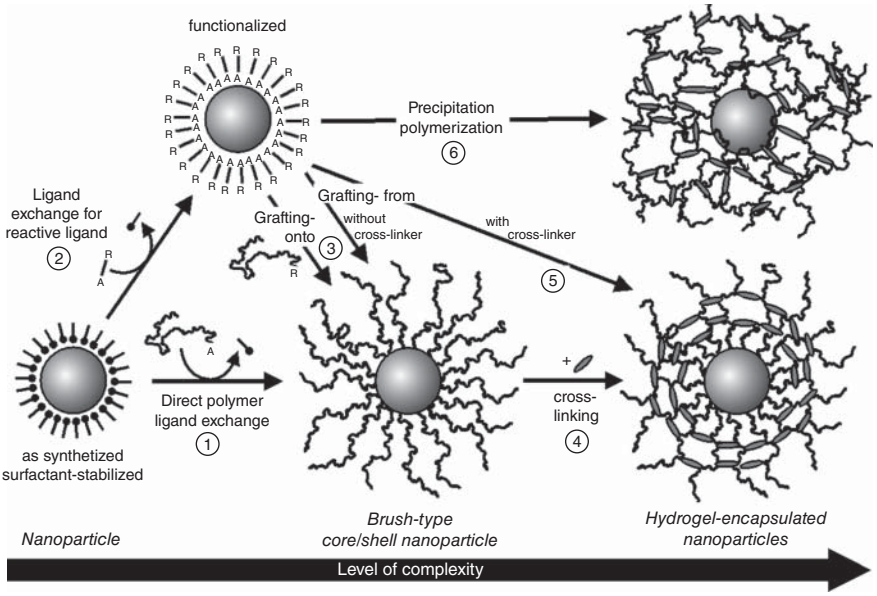

Figure 6.2 Decoration of nanoparticles with polymers with increasing level of complexity (*left to right*): As-synthetized nanoparticles are decorated with linear polymer chains by either (1) direct polymer ligand exchange or by (2) functionalization with reactive ligands and subsequent (3) polymer grafting (from/onto) to form brush-type core/shell nanoparticles. Hydrogel-encapsulation can be achieved by (4) crosslinking of brush-type core/shell nanoparticles, (5) grafting-from polymerization with crosslinker, or directly via (6) precipitation polymerization of functionalized nanoparticles. (A for anchoring and R for reactive functional group).

group serving as the anchoring group. Controlled living polymerization techniques, in particular, the atom-transfer radical polymerization (ATRP) [44], ring-opening metathesis polymerization (ROMP) [45, 46], nitroxide-mediated living radical polymerization (NMP) [47], and reversible addition-fragmentation chain transfer (RAFT) polymerization [48, 49] have proved to be very useful, since the polymerization initiator molecule can be selected such that it bears both functionalities, that is, the polymerization initiating moiety as well as the surface anchoring moiety on the same molecule.

The resulting end-functionalized polymers can be tethered to the particle surface, replacing the original stabilizing agent from the surface in a ligand exchange process. The exchange of the ligand can be driven by concentration effects when the *new* polymer ligand is presented in huge excess and/or making use of the higher binding affinity of the anchor groups of the *new* ligand. This approach yields polymer-decorated nanoparticles. Depending on the exchange protocol including the type of macromolecular ligand and the particle purification, a complete exchange can be achieved [50]. The direct polymer ligand exchange method is rather simple and allows for the precise control of the layer thickness simply by adjusting the molecular weight of the polymer during the polymer synthesis step [30, 51–54].

Brush-like polymer decoration of nanoparticles can also be achieved by growing polymers directly from the particle's surface [55]. As depicted in Figure 6.2, this *grafting-from* approach starts with the attachment of reactive molecules onto the nanoparticle surface (2). This reactive group can then be used in the subsequent polymerization of monomers (3). Such a surface-initiated polymerization yields polymer brushes of higher grafting densities with polymer chains extending outward from the nanoparticle surface. The most common polymerization techniques applied for this are again living radical polymerization techniques such as ATRP, RAFT, ROMP, and NMP, owed to their versatility toward monomers and uniform polymer growth. However, the control over the polymer chain lengths is rather difficult in comparison to *grafting-onto* method, due to the increased rate of chain growth termination caused by the high steric crowding on the particle surface. The main advantage of this technique is the facile purification of the final polymer-decorated nanoparticles via centrifugation steps [55].

The achievable interparticle distances from such polymer-encapsulated nanoparticles with brush-like polymer shells range from a few nanometers to a few tens of nanometers. Larger shell thicknesses, and hence particle separations, are accessible by gel-like polymer shells. Such gel encapsulations enable particle-to-particle separations up to hundreds of nanometers. The most prominent example for such gel networks are hydrogels, which consist of hydrophilic, crosslinked polymer networks swollen with water. The degree of swelling of a hydrogel can be enormous (>95%), and thus leads to the unique viscoelastic properties of hydrogels. In contrast to the rather small polymer brushes, the introduction of a hydrogel shell significantly increases the effective particle volume. This can be of particular interest for 3D assembly, since larger volume fractions can be achieved as compared to as-prepared nanoparticles without a thick hydrogel coating. Figure 6.2 illustrates the schematically different synthetic strategies used to obtain gel-like polymer architectures

around the particle cores. In general, *grafting-from* and *grafting-onto* approaches typically lead to core/shell particles with nanoparticle cores and brush-type polymer shells (3). If such brush-type shells are crosslinked, polymer network shells can be obtained (4). In a *grafting-from* approach, crosslinked shells can be grown directly onto the particles, simply by the addition of a bi- or multifunctional crosslinker as a comonomer in the polymerization (5). Besides these two approaches, another common approach to generate core/shell particles with hydrogel shells is based on precipitation polymerization (Figure 6.2). In this case the polymer shell is built up by precipitation of growing oligomer and polymer chains onto the nanoparticle surface (6). Reactive groups on the nanoparticle surface can chemically help to anchor the growing hydrogel to the nanoparticle. These examples only highlight the different concepts applicable to encapsulate nanoparticles by hydrogels. Additional routes may be suited for this task, for example, as in the mini-emulsion polymerization and microfluidic approaches.

The encapsulation of nanoparticles into hydrogel shells has been shown for many nanoparticle compositions, sizes, and even shapes. Already in 1994 Makino *et al*. coated poly(styrene-*co*-*N*-isopropylacrylamide) (PS-*co*-PNIPAm) latex particles with temperature-responsive shells of crosslinked poly(*N*-isopropylacrylamide) (PNIPAm) [56]. These authors synthesized the copolymer cores in a first step using a soap-free emulsion polymerization of styrene with 10 wt-% *N*-isopropylacrylamide (NIPAm) as water-soluble comonomer. The resulting latex spheres were then coated by crosslinked hydrogel shells using a seeded polymerization procedure with NIPAm and the crosslinker *N*,*N*′-methylenebisacrylamide. The final core/shell particles had single latex cores and thermo-responsive hydrogel shells homogeneously encapsulating the cores. In a very similar fashion Okubo *et al*. have synthesized core/shell particles with polystyrene (PS) and PS-*co*-PNIPAm cores, and copolymer shells composed of dimethylaminoethyl methacrylate and ethylene glycol dimethacrylate, as well as NIPAm and *N*,*N*′-methylenebisacrylamide [57]. In this work, the authors have used seeded emulsion polymerization to encapsulate the pre-synthesized latex cores. This two-step protocol resulted in core/shell particles with single nanoparticle cores and homogeneous polymer shells. Dingenouts *et al*. studied the volume phase transition behavior and the form factor of such core/shell particles using small-angle X-ray scattering (SAXS) [58]. In this particular case polystyrene core particles with hydrogel shells composed of chemically crosslinked PNIPAm were analyzed. The scattering data revealed liquid-like local concentration fluctuations of the hydrogel shell. In addition, the authors found that the linking of the hydrogel shell to the latex cores reduces the swelling capacity of the shell. At the same time, a full chain collapse at high temperatures is also prevented.

Extending the concept of seeded polymerization, Zha *et al*. have used silica nanoparticles as seed particles to yield inorganic/organic core/shell particles [59]. To guarantee a covalent attachment of the polymerizing hydrogel network onto the silica cores, these cores were functionalized with 3-(trimethoxysilyl)propyl methacrylate. This functionalization led to the formation of terminal double bonds on the nanoparticle surface. These double bonds could then be used to bind the hydrogel shell obtained by copolymerizing NIPAm with the crosslinker

N,*N*′-methylenebisacrylamide in the presence of the seed particles. The resulting core/shell particles showed the expected volume phase transition behavior of NIPAm-based hydrogels as determined by dynamic light scattering (DLS). Furthermore, the authors could show that dissolution of the silica cores allows for the preparation of hollow hydrogel shells. Following the protocol by Zha *et al*., silica cores of a broad range of sizes were incorporated into crosslinked hydrogel shells by Karg *et al*. [60–62]. These authors studied the inorganic/organic core/shell particles by different scattering techniques to investigate the swelling properties and network structure of the hydrogel shells as well as the form factor of the silica cores. Particles with a defined core/shell structure and core sizes up to 170 nm in diameter could be successfully synthesized. In all cases, the hydrogel shells showed the typical volume phase transition behavior of PNIPAm. In order to achieve core/shell particles with metal nanoparticle cores bearing a much higher refractive index than silica, the same authors have used silica-coated gold nanoparticles as core material [60]. Due to the silica coating on the gold particles, the same surface chemistry as for functionalization of pure silica nanoparticles could be applied. This way, gold/silica/PNIPAm core/shell/shell particles with thermo-responsive outer shells could be realized.

The direct encapsulation of gold nanoparticles of 17 nm in diameter into responsive hydrogel shells has been presented by Kim *et al*. [63]. These authors used surface-initiated ATRP to polymerize PNIPAm shells on gold nanoparticles. This was achieved by attaching a disulfide containing ATRP initiator on the gold nanoparticle surface. Using NIPAm as monomer and ethylene diacrylate as crosslinking comonomer, the authors were also able to produce core/shell particles with a crosslinked shell apart from brush-type core/shell particles with a non-crosslinked shell. Larger gold nanoparticle cores of 67 nm in diameter were encapsulated by shells of PNIPAm with different degrees of crosslinking by Contreras-Cáceres *et al*. [64]. In their protocol the authors used cetyltrimethylammonium bromide (CTAB) stabilized gold nanoparticles prepared in a seeded-growth fashion, and they polymerized a first layer of PS crosslinked with divinylbenzene around these cores. This first polymer layer improved the colloidal stability of the gold particles and made their surface compatible for the precipitation polymerization of NIPAm with the crosslinker *N*,*N*′-methylenebisacrylamide. The latter precipitation polymerization led to core/shell particles with thermo-responsive hydrogel shells. Furthermore, the authors demonstrated that the porous hydrogel shell allows chemical overgrowth of the gold cores. Applying different amounts of the stabilizer CTAB in the seeded-growth of the gold cores larger cores of around 90 nm in diameter with either a spherical or a star-like shape could be prepared. The same authors have also shown that the concentration of the monomer NIPAm during the polymerization can be used to realize different shell thicknesses and different crosslinking densities [65]. These parameters could be used to tune the response behavior of the core/shell particles.

A more general approach for the encapsulation of metal nanoparticles was introduced by Fernández-López *et al*. [66] These authors used a layer-by-layer strategy to coat CTAB-stabilized gold nanoparticles by an allyl-containing poly(acrylic acid).

The incorporated allyl groups could then be employed for the attachment of a hydrogel shell formed by precipitation polymerization. In this manner, the authors were able to encapsulate spherical, decahedral, and star-shaped nanoparticles into PNIPAm hydrogel shells.

Recently, Karg *et al*. have shown that gold nanoparticles of 14 nm in diameter can be homogeneously encapsulated by PNIPAm-based hydrogels without the need of an intermediate polymer coating [67, 68]. These authors have directly functionalized as-prepared gold nanoparticles with 3-butenylamine and then performed a precipitation polymerization of NIPAm with the crosslinker *N*,*N*′-methylenebisacrylamide in presence of the functionalized gold nanoparticles. Tuning the monomer feed concentration in the polymerization step and varying the crosslinker amount and addition procedure, core/shell particles with various shell thicknesses, shell morphologies, and swelling capacities were achieved.

Most examples in the literature so far employed hydrogel shells composed of NIPAm with the crosslinker *N*,*N*′-methylenebisacrylamide prepared via precipitation polymerization. Hence the resulting core/shell particles show the typical volume phase transition behavior of PNIPAm in water. This is an interesting aspect for assembly of such core/shell particles because the shell thickness becomes controllable by temperature. Also a response to pH and ionic strength can be easily programmed in the polymer shell by introducing chargeable functionalities such as carboxyl or amine groups. These groups can be introduced, for example, by copolymerization with respective comonomers. Thus, depending on the chemical composition, the physical properties of the polymer shell can be a function of external parameters such as temperature, pH, and ionic strength among others such as electric field and light. The responsiveness of such core/shell particles has led to an enormous interest in the last decades due to their potential in applications such as sensing, actuation, smart membranes, and as drug delivery systems. Since the main interest in this book chapter lies on the self-assembly of polymer-encapsulated nanoparticles, the reader is referred to these excellent review articles for further information on responsive core/shell materials and their potential applications [69–74].

6.2.2 Distance Control in 2D and 3D

As depicted in Figure 6.1, for several optical and electronic phenomena, interparticle distances in particle assemblies have to match certain well-defined length scales. Therefore, it is crucial to control the interparticle distances or pitch of nanoparticle lattices on surfaces or in bulk matrices. Molecular and macromolecular ligands allow for covering interparticle spacings between 1 nanometer and several 100 nanometers (see Figure 6.3A). Here the main parameter in order to control the distance in 2D and 3D assemblies is the thickness of the macromolecular corona.

Directly from synthesis, small-molecule stabilizers such as citrate yield interparticle distances of only 1 nm. Figure 6.3B shows a colloidal monolayer of 14 nm-sized gold nanoparticles crystallized into hexagonally close-packed lattices [75]. The spacing corresponds well with the size of two overlapping citrate molecules in-between

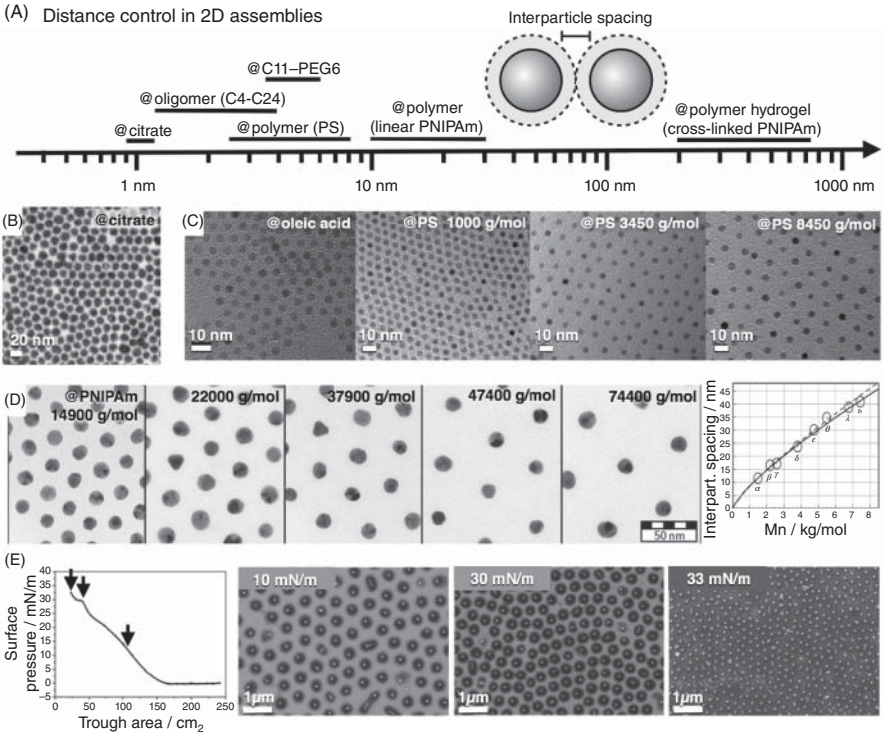

Figure 6.3 Distance control in 2D assemblies: (A) Length scale of interparticle spacings with corresponding examples of macromolecular ligands: citrate (from synthesis), short chain oligomers/surfactants, surfactant–polymer hybrids, linear polymers of different molecular weights, and hydrogel shells. (B) As-synthesized citrate-stabilized gold nanoparticles. Adapted with permission from [75]. Copyright 1993 ACS. (C) Fe_3O_4 nanoparticles with oleic acid and modified with PS ligands. Adapted with permission from [26]. Copyright 2014 ACS. (D) Gold nanoparticles with shells of linear PNIPAm ligands. Adapted with permission from [76]. Copyright 2013 ACS. (E) Ordered arrays of gold nanoparticles with crosslinked PNIPAm shells assembled at the air/water interface at different (transfer) surface pressures. Surface pressure-area isotherm and corresponding monolayer assemblies after transfer to solid substrates. Adapted with permission from [77]. Copyright 2012 ACS .

two particles separated by steric repulsion, if all three carboxyl groups are coordinated toward the surface [75].

To increase the spacing, the original ligand shell can be substituted for oligomeric ligands, which are surfactants with chain lengths of up to twenty carbons. Consequently interparticle separations with oligomeric ligands are inherently limited by their short persistence length and their inherent tendency to intercalate when situated in close contact. Especially in the longer alkyl chains with coordination groups of moderate binding affinity, some interpenetration of contacting ligands may occur, leading to a decrease in the interparticle spacing. Thus surfactants can provide spacings up to about 4 nm [78]. The interparticle separation increases linearly

with the number of CH_2 groups, though the size of the head group and of the methyl-terminating group should be taken into account [75]. The surfactant-oligomer hybrids, composed of a short oligomeric anchoring chain (HS-$C_{11}H_{22}$-) and a small number of repeating units of poly(ethylene glycol) (-PEG_6-COOH), can only provide for about 4–6 nm of spacing [79]. Larger separations inherently require a transition from oligomers to polymers.

Figure 6.3C shows the application of PS ligands to widen the interparticle gaps in a colloidal 2D assembly of 5 nm-sized Fe_3O_4 nanoparticles [26]. The first TEM image shows the iron oxide particles with their original oleic acid corona, as received from synthesis. The next images show assemblies of the same core particles but with PS ligands of different molecular weights (M_n = 1000, 3450, and 8450 g/mol) introduced by direct polymer ligand exchange using poly(ethyleneimine) anchors. Here the shortest PS spacer with merely 1000 g/mol, which corresponds to about 10 repeating units, shows an even smaller particle spacing (7.2 nm) than the original stabilizing corona of oleic acid. Only when the ligands become significantly longer, 30 and 80 repeating units, the 2D spacing increases to about 8–10 nm [26]. In order to yield well-defined and controllable distances, the ligand corona has to be dense and homogeneous [26, 80].

Another example of molecular-weight-dependent changes in spacing is shown in Figure 6.3D. Ebeling and Vana prepared 14 nm-sized gold nanoparticles with linear PNIPAm chains prepared by RAFT polymerization [76]. The resulting self-assembled lattices of gold cores show interparticle spacings from 11 to 41 nm, depending on the molecular weight of the ligand. The authors indicated that the spacing does not increase strictly linear with increasing molecular weight of the PNIPAm ligand (see Figure 6.3D, plot to the right). The observed deviation from the model is due to imperfections of the (partially coiled) polymer brush and variations in the grafting density. Besides the end-tethered ligands, the authors presented also ligand motifs resulting in more complex (e.g., crosslinked) binding scenarios [76].

One might expect that the step toward even wider spacings can be simply done by further increasing the size of the polymeric ligands. However, at high molecular weights the binding strength of only one anchoring group may not suffice to keep the polymer chain tethered to the particle surface [81]. Pletsch *et al*. reported on Ag particles modified by direct polymer ligand exchange of the original poly(vinylpyrrolidone) (PVP) shell for thiol-terminated PS chains with six different molecular weights between 21,200 to 217,200 g/mol [82]. Especially for higher molecular weights, a tendency toward aggregation was found even though the NMR results and elementary analysis indicated a quantitative ligand exchange. This colloidal instability may result from the irreversible desorption of the polymer ligand from the particle surface, owed to the imbalance of ligand size and anchoring strength (Au-thiol binding) above a threshold molecular weight.

In order to achieve homogeneous particle arrays of larger spacing, this colloidal instability needs to be avoided. As already discussed in the previous section, one measure to counteract such instabilities is to crosslink the ligand shell forming a stable core/shell particle. Karg *et al*. have shown that monolayer of gold/PNIPAm

core/shell particles can be prepared by different methods such as spin-coating [83]. Using hydrogel shells of two different thicknesses, the authors show that the surface coverage of gold nanoparticles can be tuned. The monolayers were characterized by imaging as well as by spectroscopic techniques. The optical properties of the monolayer studied by ellipsometry revealed a larger area fraction of gold particles for the monolayer prepared from core/shell particles with thinner hydrogel shells. Hence, it could be shown that the hydrogel shell allows adjustment of the interparticle separation of the nanoparticle cores.

Capitalizing on the soft properties of hydrogels Vogel *et al*. achieved a gold nanoparticle monolayer with different interparticle distances using a Langmuir–Blodget approach [77]. These authors used gold cores of 60 nm in diameter homogeneously encapsulated in a soft PNIPAm hydrogel shell by precipitation polymerization. Figure 6.3E shows ordered 2D assemblies of the Au@PNIPAm gel particles, which were assembled at the air/water interface and transferred onto solid substrates. Due to the deformability of the soft hydrogel shell, spacings of 650–300 nm, controlled by the surface pressure, could be obtained. The hexagonal ordering is preserved throughout the isotherm and even after transfer of the monolayer onto substrates allowing for precise tuning of the interparticle distances.

Recently, Clara-Rahola *et al*. have shown that the temperature sensitivity of PNIPAm can be used to tune the surface coverage of 2D arrays of PNIPAm-encapsulated gold nanoparticles [84]. In this work the particle arrays were prepared by drop-casting and drying the dilute particle dispersions on indium tin oxide (ITO)-coated glass substrates at different temperatures. The authors showed that the polymer shells can be removed by post-treatment of the particle arrays with plasma etching, hence allowing the preparation of a metal nanoparticle monolayer with tunable interparticle separation.

The effect of surface charge on the assembly of core/shell particles with PS cores was investigated by Lu *et al*. [85]. Core/shell particles with positive and negative surface charge were prepared by simply changing the type of radical initiator used in the polymerization of the hydrogel shell. Ordered structures were obtained for assemblies of charged particles on oppositely charged substrates; however, the degree of order was significantly lower for substrates with an equal sign of charge.

Apart from distance control in two dimensions, the self-assembly can be extended to 3D organizations [87]. Due to the relatively large dimensions of hydrogel shells employed for encapsulating nanoparticle cores, the effective particle volume is strongly increased. This significantly lowers the amount of material needed to achieve volume fractions, which are above the crystallization threshold. Karg *et al*. have studied the phase behavior of gold nanoparticles with PNIPAm hydrogel shell and identified a large range of concentrations where crystalline samples are found [86].

Figure 6.4A shows a self-organized colloidal crystal of such core/shell particles. The hexagonal packing and high degree of order can be depicted from the shown electron micrograph. For studying the crystal structure of 3D assembled polymer-encapsulated nanoparticles, small angle scattering experiments are ideally

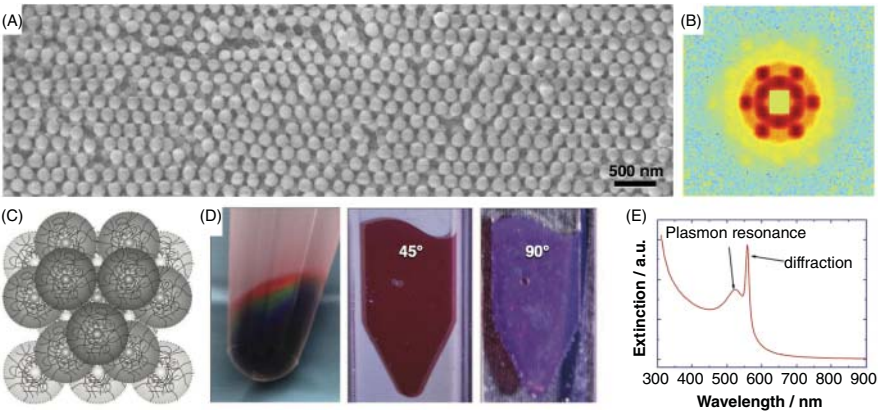

Figure 6.4 Distance control in 3D assemblies: (A) SEM image of a colloidal crystal of gold nanoparticles with shells of crosslinked PNIPAm prepared by precipitation polymerization [Karg *et al*., unpublished data]. (B) 2D detector image from small-angle neutron scattering of a crystalline Au/PNIPAm core/shell sample measured on the D11 instrument of the Institute Laue–Langevin at a sample-to-detector distance of 28 m [Karg *et al*., unpublished data]. (C) The pronounced Bragg peaks can be attributed to a face-centered cubic structure [86]. (D) Photographs of the crystalline samples under different angles of illumination [86]. The strong Bragg diffraction can be seen with the naked eye. (E) UV/vis extinction spectrum of a photonic crystal of gold/PNIPAm core/shell particles showing the typical localized surface plasmon resonance of spherical gold nanoparticles and a diffraction peak [86]. (C–E) Adapted with permission from [86]. Copyright 2011 Wiley. (*See color insert for color representation of this figure*).

suited. Figure 6.4B shows a 2D detector image obtained from small angle neutron scattering (SANS) investigation of a colloidal crystal of hydrogel encapsulated gold nanoparticles. The detector image shows strong Bragg peaks, indicating the high degree of order in the colloidal crystal. In this particular case, the Bragg peaks correlate well with a face-centered cubic lattice (Figure 6.4C). For sufficiently large lattice constants, achieved by large hydrogel shell thicknesses, such crystals are characterized by strong and narrow diffraction peaks, which are located in the visible wavelength range. As shown in Figure 6.4D, the crystalline sample exhibits a strong purple iridescence upon top illumination (90°), whereas at an incident angle of 45° the reflection appears deep red. The UV/vis extinction spectra reveal the typical localized surface plasmon resonance of the gold cores (519 nm) and the lattice diffraction (560 nm). Increasing the volume fraction led to a blue shift of the diffraction peak due to a decreasing lattice constant [86]. Furthermore, the authors have shown that temperature can be used to melt and anneal the crystals, due to the volume phase transition behavior of the thermo-responsive PNIPAm shell.

The examples in this section have illustrated that polymer decoration of nanoparticles enables the preparation of 2D and 3D assemblies where the polymer shell thickness can be employed to control the interparticle distance. Furthermore, it was shown that the soft and deformable properties of polymers allow for the

reduction of the interparticle separation when for example the volume fraction is increased. The control of the particle gap is prerequisite for the development of optically functional materials that show, for example, strong coupling to external electromagnetic fields as a consequence of collective plasmonic oscillations [87]. As a result, frequency-selective responses of high spectral quality are achievable. Such features increase the potential of colloidal crystals as well as other examples of 3D assemblies like composite and inverse opals to open up new pathways to sophisticated photonic applications [88].

6.2.3 Breaking the Symmetry

After the discussion of macromolecule-guided self-assembly to fabricate close-packed structures in 2D and 3D, the following section will focus on the controlled formation of linear assemblies. The means by which the aggregation of nanoparticles can be directed toward the formation of chains and rings is by breaking the symmetry.

Figure 6.5A introduces the concept of employing the reversibility of surface coordination for controlled aggregation. Ehlert *et al*. showed that reduction of the ligand excess in the direct polymer exchange may result in formation of short multiplet chains and percolated networks from 4 nm CdSe particles stabilized by PS ligands [26]. Following the mass action law, the substitution of ligands is determined by the ligands' binding affinities (equilibrium-binding constant K) and the available ligand concentrations at the particle surface and in solution. Therefore the stability of polymer-stabilized nanoparticles can be reduced in a controlled fashion by using ligands with lower binding strength and/or reducing the excess of the polymer ligands in the ligand exchange [26]. An alternative approach is the application of a competing ligand with higher binding affinity in order to reduce the brush density at the particle surface and thus its colloidal stability.

Kumacheva *et al*. reported on the assembly behavior of bifunctional nanoparticles site-specifically functionalized with low- or high-molecular-weight ligands [89]. Figure 6.5B shows gold nanorods with a surfactant bilayer of CTAB at the longitudinal side and PS end-caps at both ends. The end-caps consist of thiol-terminated linear PS chains of 12,000 g/mol, which were attached by partial ligand exchange based on different crystallographic facets of gold [89]. Upon aggregation in a selective solvent mixture, such amphiphilic nanoparticles form linear aggregates by end-to-end aggregation. However, bifunctionality is not mandatory to break the symmetry in nanoparticle self-assemblies, and also nanoparticles with an isotropic/uniform macromolecule form linear end-to-end assemblies.

Figure 6.5C shows the solution-based self-assembly of silver nanocubes and spheres into dimers and linear oligomers [90]. The 50 nm-sized nanoparticles were stabilized by thiol-terminated PS ligands of 5,000 g/mol attached by ligand exchange. The self-assembly upon controlled aggregation was triggered by the reduction of the solvent quality for PS. Surprisingly, predominantly linear aggregation takes place. End-on attachment was explained as due to attractive hydrophobic/poor solvency forces and repulsive electrostatic forces of charged nanoparticles in a

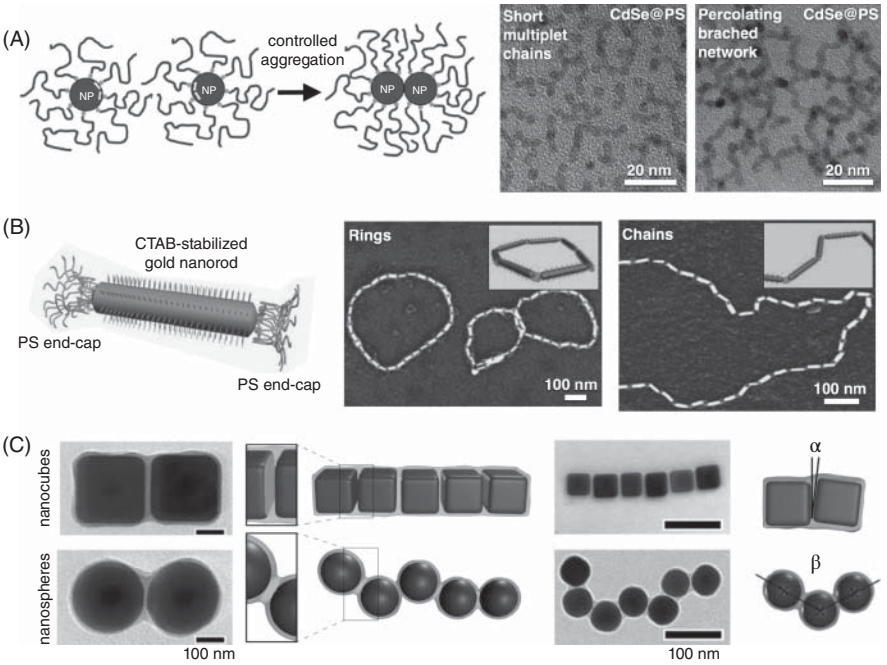

Figure 6.5 Controlled aggregation of polymer-decorated nanoparticles into linear assemblies: (A) Controlled aggregation of CdSe nanoparticles decorated with PS brushes forming short chain multiplets and percolating branched networks. Adapted with permission from [26]. Copyright 2014 ACS. (B) Self-assembled rings and chains of PS end-capped CTAB-stabilized gold nanorods in selective solvents. Adapted with permission from [89]. Copyright 2007 NPG. (C) TEM images of self-assembled dimers and linear chains of nanocubes and nanospheres with PS ligands. The schematic depictions show the contact situation and define the contacting angle α for cubes and β for sphere assemblies. Adapted with permission from [90]. Copyright 2014 ACS.

solvent with a high dielectric constant. In comparison to nanospheres, nanocube assemblies exhibited significantly higher collinearity because of the preferential face-to-face configuration that allows for larger contact areas and/or overlap volumes of two ligand shells in contact (see Figure 6.5C). The authors found that 75% of neighboring cubes show a junction angle α, the angle between the faces of the adjacent cubes, of less than 10°. Face-to-face orientation provides the maximum screening of interactions of PS with the poor solvent. By reducing the particle size to 25 nm but using the same PS ligand, the junction angle is increased significantly (only 30% with $\alpha < 10°$) and thus reduced face-to-face orientation. Regarding longer nanoparticle oligomers, this trend translates to a high collinearity for nanocube assemblies (70%, $\beta > 160°$). Consequently, nanosphere assemblies suffer from the small contact area/overlap volume and show higher tendency to bend or form kinks (45%, $\beta > 160°$) independent of the particle-to-shell size ratio [90].

6.3 GUIDING ASSEMBLY BY DECORATION WITH BIOMACROMOLECULES

While we have focused on nanoparticle modification by artificial macromolecules in the previous chapter, we will now turn our attention toward biomacromolecules, which are of particular interest for further increasing structural, chemical, and biological complexities. Biological molecules exhibit extremely well-defined molecular structures, shapes, and chemical activity as a result of the defined placement of specific functional groups in space and in time. Consequently, hierarchical 3D structures from molecular scale to macroscale and complex enzymatic cascade reactions are achieved. These features have motivated many researchers of different scientific communities to take advantage of the complexity already present in these materials and manipulate them for directing the formation of intricate nanostructures. Thereby, the physicochemical interactions in these biological macromolecules that give rise to the structural and functional diversity in nature are adopted for guiding the self-assembly of colloidal nanoparticles because of their specificity and programmable nature [91]. The two main classes of such biological macromolecules are the polynucleic acids (DNA and RNA) and polypeptides (proteins, enzymes). In the following, we will discuss the strategies to show how nanoparticles can be decorated with such biopolymers to subsequently induce self-assembly into sophisticated nanostructures in 2D and 3D.

6.3.1 DNA-Assisted Assembly

DNA-assisted assembly has opened a wide field of well-defined nanostructures due to the unique properties of DNA, in particular its specific base-pairing interactions known as the Watson–Crick base-pairing [92]. Figure 6.6A shows a schematic representation of an unfolded paired strand of DNA coordinated by the local interactions of its four building blocks (adenine, thymine, guanine, and cytosine) that are translated into the characteristic double helical structure and folding. Here the nucleic base adenine pairs exclusively with thymine, and guanine pairs with cytosine via intermolecular hydrogen bonds (see Figure 6.6B), allowing for highly specific recognition and reversible bonding [92, 93].

Seeman [93] was one of the first researchers in the DNA technology field who suggested DNA as a structural material for self-assembly using base-pairing interactions [92]. By programming structural design in the DNA and using them as DNA scaffolds or site-recognition entities, complex DNA-assisted nanoassemblies can be obtained [96–102]. The basic concept for DNA-assisted assembly of nanoparticles comprises of attaching a DNA single strand orthogonally to a nanoparticle surface and hybridizing it with a complementary strand, which is attached to another particle or surface [103]. In 1996, Mirkin *et al*. and Alivisatos *et al*. were the first researchers who used DNA-hybridization to assemble nanoparticles into nanoparticle arrays [94] and distinct dimers and trimers [95]. They applied thiol-functionalized complementary strands of DNA and attached them to different gold nanoparticles, owed to the thiophilic character of gold (see Figure 6.6C). In this respect, DNA strands with terminal

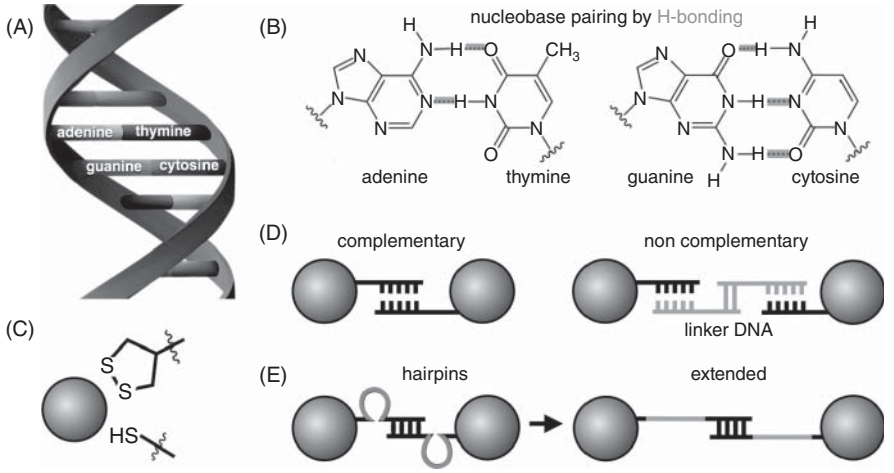

Figure 6.6 Principles of DNA ligation and hybridization as schematic representations: (A) Helical segment of double-stranded DNA with (B) Watson–Crick base-pairing. (C) Decoration of nanoparticles by ligands with terminal thiols of disulfides. (D) Hybridization strategies utilizing single-stranded DNA: direct linking of complementary ligands versus hybridization of noncomplementary ligands via a linker segment. (E) Simplified transition of hairpin segments into extended DNA ligands [94, 95].

thiol or disulfide proved to be the most applicable for ligation on gold nanoparticles. Consequently, the nanoparticles with the complementary strands could be assembled upon the hybridization of the DNA strands (see Figure 6.6D). In general, two hybridization strategies found application: (1) nanoparticle decoration with complementary strands for selective but immediate coupling (Figure 6.6C); and (2) nanoparticle decoration with noncomplementary strands, which require an additional linker strand with the respective inverse motifs as a mediator (Figure 6.6D). The latter strategy, upon application of distinct linker agents, allows for highly selective addressing of specific nanoparticles based on their ligation. Hairpin segments bring additional functionality for structural control. Hairpin loop segments arise from back folding a single strand of DNA, owing to intrastrand base-pairing of complementary base regions. The resulting loop structure is a key feature in the folding of RNA secondary structures. Upon unpairing, such hairpin loops allow for the subsequent extension of ligand-coordinated assemblies, yielding variations of interparticle separations (see Figure 6.6E) [94, 95].

Since then, a huge number of different approaches for the fabrication of nanostructures by DNA self-assembly were developed [96–102]. Simple as well as complex 2D and 3D nanostructures such as oligomeric nanoparticle chains [104], chains of nanoparticle pairs (tetramers and hexamers) [105], 3D networks, nanoparticle assemblies in triangular [106], square [106], hexagonal [107], and chiral configurations [108] have been reported. In addition, particle assemblies in core/satellite nanostructures consisting of a central nanoparticle linked to satellite nanoparticles were also

achieved by DNA-hybridization approaches. Here the core and the satellite particles can be varied in their material composition such as by semiconductor quantum dots [109] or metals such as gold or silver nanoparticles [110, 111], and in shape such as isotropic and anisotropic [112, 113]. For the DNA decoration of the various nanoparticles, ligation strategies vary from single thiol and dithiol bonds for metal and semiconductor particles and classical amide bonds using amine and activated carboxylic groups [103]. The combination of the nanoparticle building blocks can be performed in dispersion or on functionalized substrates. For example, core/satellite nanostructures consisting of a gold core and gold satellites [114, 115], silver core and gold satellites [110, 116], and semiconductor quantum dot core with gold satellites were obtained in dispersion, using DNA [109].

Besides the configurational and compositional variations, also switchable and reconfigurable assemblies can be achieved using sophisticated DNA designs and combinations. Using hairpin-structured DNA, reconfigurable and switchable Au-core/Au-satellite nanoclusters are obtained, where the interparticle distance between the core and the satellite nanoparticles can be changed. The DNA-tether between the particles was designed to assemble in a compact (hairpin) state and to reconfigure to an extended state by activated strand substitution. These types of nanoassemblies can be used as molecularly driven plasmonic switches [110, 115].

Interparticle distances in DNA assisted assemblies can also be tuned by using DNA of various lengths. For example, Cheng *et al*. have employed such a DNA-based route to create freestanding nanoparticle superlattices (see Figure 6.7A) [117]. The authors have capped gold nanoparticles of 13 nm in diameter with single-stranded DNA using thiol-linkers and were able to prepare freestanding nanoparticle films trough dewetting on a microhole substrate. Using DNA strands of different lengths, the authors were also able to tune interparticle distance within the nanoparticle sheets. Although DNA is solely used as a ligand here and base-pairing was not involved in the lattice formation, this example nicely shows how DNA can be used as a versatile capping agent to achieve homogeneous, ordered nanoparticle structures with large dimensions [117].

Figure 6.7B shows the pH-responsive core/satellite assemblies for use in living cell plasmonic imaging. These nanostructures/clusters are assembled from a complementary recognition of binary gold nanoparticles. The coupling of 50 nm cores carrying a guanidine-rich motif ligand and the satellites (14 nm in diameter) with the inverse motif (see Figure 6.7B, bottom left) was archived avoiding the formation of macroscopic aggregates (core : satellite = 1:200, at pH 8) [118]. Upon assembly, a red shift of the LSPR of 14 nm relative to that of the initial Au core nanoparticle dispersion was observed. Upon changing the pH to 5.0, the LSPR band showed a sharp blue shift, indicating the release of satellite nanoparticles (disassembly). The pH-triggered assembly and disassembly was also monitored by measuring scattering spectra from single nanoclusters [118].

The DNA-assisted approach was also used to combine different shaped nanoparticle building blocks. Core/satellite nanoclusters consisting of a triangular Au nanoprism core and spherical Au satellites were reported [112]. Asymmetric gold Janus nanoclusters were synthesized by a stepwise surface-encoding protocol. The

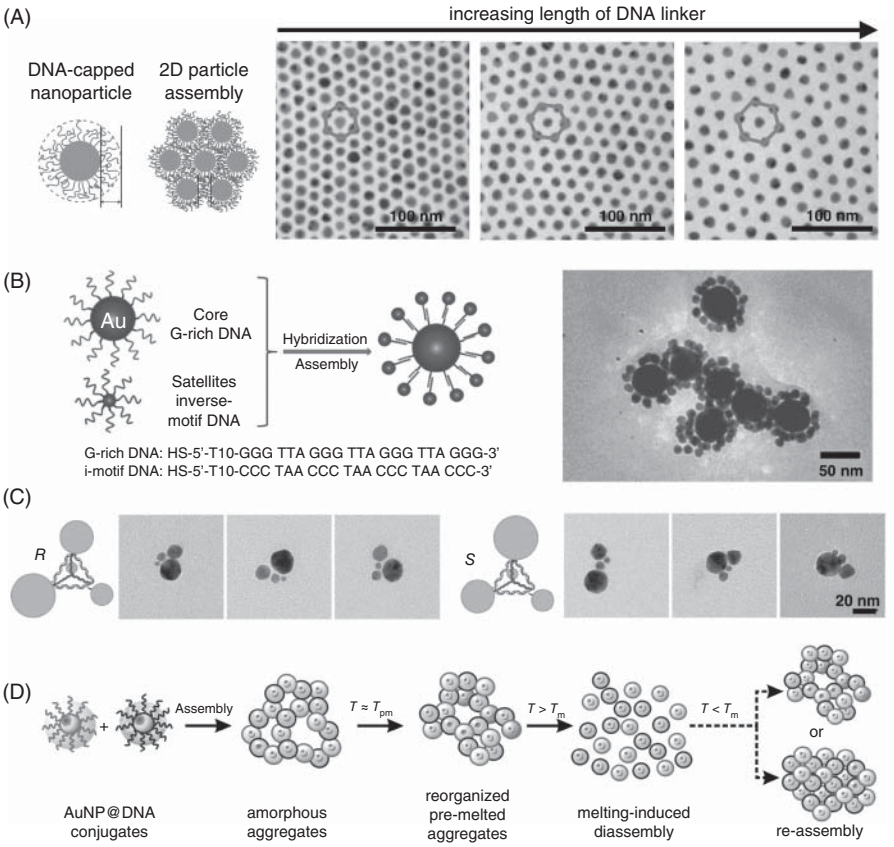

Figure 6.7 Examples of DNA-mediated assembly of nanoparticles upon DNA hybridization: (A) Distance control in freestanding superlattices of gold nanoparticles capped with DNA linker of variable length. Adapted with permission from [117]. Copyright 2009 NPG. (B) core/satellite structures of particles functionalized with complementary DNA ligands. TEM image show the dense population of satellites around the core particles. Adapted with permission from [118]. Copyright 2013 RSC. (C) Chiral pyramids of DNA-nanocrystal conjugates. TEM images show that the assembled enantiomers exhibit different chirality (left *R*, right *S*). Adapted with permission from [108]. Copyright 2009 ACS. (D) DNA-guided amorphous aggregation and subsequent reorganization into nanoparticle crystals. Adapted with permission from [119]. Copyright 2008 NPG.

predominant penta-valent core/satellite structures were obtained after different immobilization (on functionalized substrate), hybridization, and release steps using different sized DNA-encoded Au nanoparticles [111, 120].

Figure 6.7C shows chiral pyramids of DNA-nanoparticle conjugates using gold nanoparticles. Initially, when nanoparticles of equal sizes join, pyramidal assemblies are formed. The pyramidal geometry was confirmed by SAXS. The use of specific DNA ligands allows for control over the spatial position and order of these nanoparticles. Consequently, by joining tetraeders of nanoparticles that all differ in size, chiral

nanostructures are feasible. The corresponding TEM images show the successful assembly of enantiomers of different chirality (left *R*, right *S*) [108].

Figure 6.7D shows the DNA-guided crystallization of binary nanoparticles into aggregates of variable long-range order. Gold nanoparticles with complementary DNA decorations were assembled by hybridization into mesoscale aggregates. At room temperature, an initially amorphous phase of DNA-linked aggregates is formed upon recognition. At elevated temperatures, a melting-induced disassembly of the amorphous aggregates may be induced. Upon subsequent cooling, the system either falls back to its unordered amorphous phase or experiences spontaneous crystallization. This suggests a coexistence of reorganized densely packed particles, which may act as nuclei for crystal growth, and unassembled particles. By thermal cycling, crystalline aggregates with remarkable long-range order could be produced. This temperature-triggered reversible hybridization/dehybridization of DNA allows 3D networks of nanoparticles to be modulated and reconfigured. Reversible aggregation can provide for structural and compositional control in ordered 3D nanoassemblies [119].

In conclusion, DNA-assisted self-assembly is highly selective and offers the possibility to fabricate well-defined nanoparticle assemblies of variable interparticle distances in a variety of complex structures. Moreover, the possibility to use reconfigurable or stimuli-responsive DNA-based linkers makes this method interesting for several applications. However, this assembly method is poorly scalable and requires high cost synthesis routes, making this method less feasible in applications.

6.3.2 Protein-Assisted Assembly

In comparison to DNA and RNA, proteins are another class of biopolymers that are highly diverse and embed hierarchically many layers of molecular and structural organization. Proteins are macromolecules consisting of 21 different monomers, namely amino acids with hydrophilic and hydrophobic residues bond into a polypeptide chain. In order to minimize the conformational energy of individual amino acid residues in the chain, to maximize hydrogen bonding of polar groups, and to bury hydrophobic residues away from the aqueous environment, these chains fold and organize into highly ordered 3D architectures. The folded proteins can further self-assemble upon molecular recognition to protein superstructures and protein complexes, giving rise to unique functional entities such as transmembrane pumps and molecular motors [121].

Hence proteins and protein structures have been widely employed to assemble colloidal nanoparticles, and used either as scaffolds or recognition entities (Fischer's key–lock principle) [122] for guiding nanoparticle assemblies. In the following, we will discuss different strategies and requirements for decorating colloidal particles with proteins that can be used in their 2D and 3D assemblies. In general, there are three main principles for the protein decoration of nanoparticles that find application in protein-assisted assembly of nanoparticles: covalent binding (Figure 6.8A), peptide affinity binding (Figure 6.8B), and physisorption (Figure 6.8C).

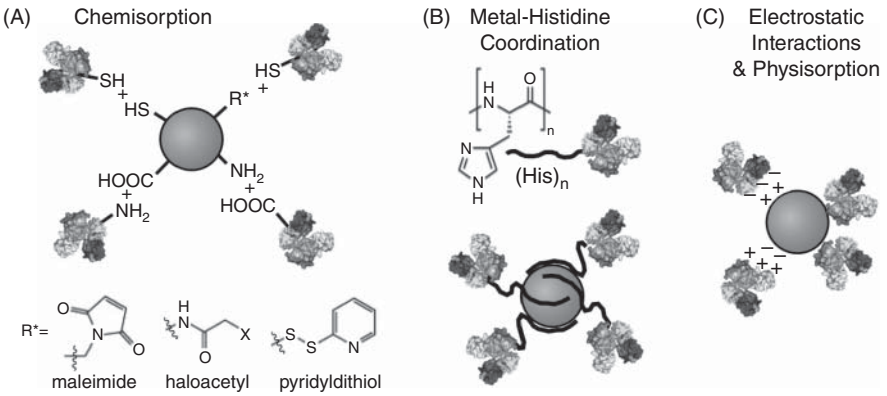

Figure 6.8 Principles of protein decoration of nanoparticles as schematic representations: (A) Chemisorption upon covalent bonding. (B) Metal-histidine coordination of proteins with polyhistidine tags. (C) Electrostatic adsorption and physisorption of proteins.

For attaching proteins covalently to nanoparticles (Figure 6.8A), the nanoparticle has to be first decorated with chemical functionalities such as carboxylates, amines, alcohols, and thiols that enable protein attachment via organic coupling reactions, yielding chemical bonds such as amides, esters, thioethers, and disulfide bonds, respectively, between the particle coating and the protein [123, 124]. However, due to the colloidal instability issues related to nanoparticles and the protein denaturation problems under reaction conditions that are beyond the ideal conditions for proteins, only few coupling reactions can be employed. The most applied reaction is the amide coupling reaction, where primary amine group (-NH_2) reacts with an activated carboxylic acid (-COOH) group in aqueous media. For the activation of the carboxylic acid group carbodiimide compounds provide the most popular and versatile method. The most readily available and commonly used carbodiimides are the water-soluble EDC (1-ethyl-3-(-3-dimethylaminopropyl) carbodiimide hydrochloride) for aqueous crosslinking and the water-insoluble DCC (*N*′,*N*′-dicyclohexylcarbodiimide) for nonaqueous organic synthesis methods. *N*-hydroxysuccinimide (NHS) or its water-soluble analogue (sulfo-NHS) is often included in carbodiimide coupling protocols to improve efficiency or create dry-stable (amine-reactive) intermediates. The amine coupling reaction is highly versatile in regard to proteins and particles types, since proteins bear both amine and carboxylic groups and nanoparticles can be easily decorated with amine or carboxylic functionalities. Besides amine-coupling reactions, sulfhydryl-reactive chemical groups such as maleimides, haloacetyls, and pyridyl disulfides (Figure 6.8A, bottom) can be used for attaching proteins covalently to nanoparticles. The proteins are then covalently attached to nanoparticles via thioether or disulfide bonds, respectively [124].

The second most applied strategy for decorating particles with proteins or peptides makes use of metal affinity binding entities such oligohistidine tags (*His-tags*), which have a high binding affinity toward metal surfaces (Figure 6.8B) [124]. Such *His-tags*

are engineered biotechnologically or genetically into the protein sequence. Peptide synthesizers (solid phase) or the above-mentioned coupling reactions (liquid phase) can also be used to add a *His-tag* to peptide sequences. Finally, such *His-tag*-labeled proteins attach to nanoparticles, with the *His-tag* attaching preferentially to the particle surface. The nanoparticles that can be employed are usually metal nanoparticles, due to the high affinity of *His-tags* toward metals. However, the method is costly and yields a very low amount of labeled proteins, owed to the multiple and arduous protein engineering steps.

The third method of decorating nanoparticles with proteins comprises simply the physisorption of proteins onto nanoparticles using electrostatic and van der Waals forces (Figure 6.8C). Proteins readily adsorb onto nanoparticles forming an undefined protein layer, the so-called protein corona on any type of nanoparticle system. However, if metal nanoparticles are employed, the protein layer adsorbs strongly onto the metal surface, yielding a robust protein coating [125–128].

Once immobilized onto nanoparticle surfaces, such protein-decorated nanoparticles can be guided to self-assemble into complex structures via their inherent specific interactions. One of the prominent specific interactions of proteins is based on the bio-recognition principle, where the host protein binds a guest molecule or another protein or peptide with high specificity. This binding principle is often referred to host–guest or key–lock principle [122]. Figure 6.9 shows some of the widely applied systems, including biotin–streptavidin (Figure 6.9A) [129], enzyme-inhibitor (protein–protein) (Figure 6.9B) [130], aptamer–thrombin (oligopeptide–protein) (Figure 6.9C) [131], and carbohydrate–lectin (carbohydrate–protein) (Figure 6.9D) interactions [132]. Figure 6.9A and C show examples of gold nanorods functionalized with end-thiolated biotin or aptamer molecules at the nanorod tips, respectively. Upon addition of the multivalent host protein streptavidin or thrombin, respectively, the gold nanorods assemble tip-to-tip in longer particle chains. By attaching the guest and host molecules on different particle types, multi-component assemblies can be achieved. Figure 6.9B shows an example where a host protein (Barnase) is attached to magnetic nanoparticles and the guest protein (Barstar) to a quantum dot. Upon adding the Barstar-decorated quantum dots in excess to the Barnase-decorated nanoparticles, the quantum dots arrange on the magnetic nanoparticles in a core/satellite structure. It is worth noting that the decoration of nanoparticles with proteins and their assembly can also be achieved, via immobilizing the guest molecules (biotin, inhibitor protein, aptamer, carbohydrate; see Figure 6.9A–D) onto the nanoparticles and then locking the host protein onto the immobilized guest molecule. By adjusting the molecular ratio of the immobilized guest and free host molecules, protein decoration or particle assembly can be achieved for low or high ratios, respectively. Figure 6.9D shows an example for the latter case. Here the nanoparticles are decorated with α-D-mannosyl or α-D-glucosyl residues (guest molecule), and upon adding the host protein concanavalin A (ConA) at relative low ratios, the particles assemble into 3D nanoparticle networks.

For the colloidal assembly of nanoparticles in dispersion (3D) and on substrates (2D), it is critical that the functional coatings are robust and comply with such prerequisites as high colloidal stability, high concentration, tunable surface wettability,

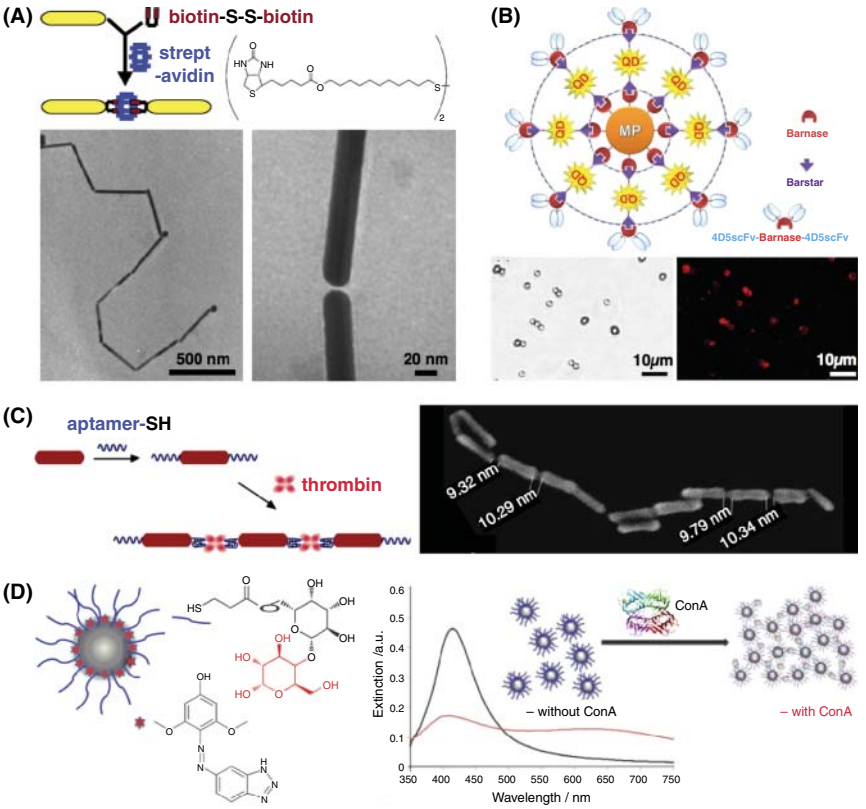

Figure 6.9 Examples of protein-mediated assembly of nanoparticles: (A) End-to-end assembly (linear aggregation) of gold nanorods tip-functionalized by biotin disulfide with streptavidin as linker. TEM images showing tip-to-tip aggregation of nanorod chains. Adapted with permission from [129]. Copyright 2003 ACS. (B) Superstructure of a magnetic core particle (MP), quantum dots (QD), and superfacial tags (4D5scFv-Bn) utilizing the key–lock type bio-recognition of two proteins (Barstar/Barnase). Bright-field (*left*) and fluorescence microscopy images (*right*) showing trifunctional nanoparticle assemblies. Adapted with permission from [130]. Copyright 2010 PNAS. (C) End-to-end assembly of gold nanorods tip-functionalized with a thiolatedaptamer with thrombin as linker. TEM image with selected tip-to-tip distances. Adapted with permission from [131]. Copyright 2009 ACS. (D) Mixed monolayer assembly by aggregation of glyco-decorated nanoparticles using a protein (ConA) as linker. UV/vis extinction before and after the addition of ConA. Adapted with permission from [132]. Copyright 2013 RSC. (*See color insert for color representation of this figure*).

and stimuli-responsiveness. Defined protein coatings on metal nanoparticles have revealed a facility to fulfill most of these requirements, thus enabling controlled modular assemblies [133] in dispersion and highly ordered, macroscopically scaled particle assemblies on substrates, for example, as shown recently by Hanske *et al*. [128] for nanospheres and Tebbe *et al*. [134, 135] for nanorods.

6.4 APPLICATION OF ASSEMBLIES

The previous sections provide scientists with a set of tools for gaining control over structural features of nanoparticle assemblies. As highlighted in Figure 6.1, optical and electronic properties correlate strongly with interparticle distances. In the following we will illustrate, with some selected examples for the case of plasmonic nanoparticles, how optical properties can be tuned in the assemblies.

In particular, plasmonic coupling between nanoparticles is highly sensitive to variations in particle spacing, orientation, and material composition. Thus, applications of macromolecular ligands as agents to direct the assembly of clusters or arrays of plasmonic nanoparticles are already found in optical sensing and nonlinear nanophotonics.

Pazos-Perez *et al*. have prepared highly symmetric plasmonic nanoparticle clusters with coordination numbers (CN) up to 7 (see Figure 6.10A), and these clusters were separated by density gradient centrifugation [136]. The authors used a macromolecular linker of poly(ethylene oxide)-*b*-poly(propylene oxide)-*b*-poly(ethylene oxide) (PEO-*b*-PPO-*b*-PEO) introduced by direct polymer ligand exchange to substitute the original surfactant shell of CTAB. The clusters were formed by gradual evaporation of toluene from emulsion droplets of aqueous nanoparticle dispersions with toluene [138]. The decrease in volume yields highly symmetric assemblies of closely assembled nanoparticles with interparticle separations of about 2 nm. Compared to DNA or other organic linkers, polymers exhibit lower Raman cross sections [139]. Therefore polymer linkers are preferable for assemblies for SERS application because analytes can be concentrated within close proximity of the particle surface while vibrational signal contamination is avoided [136]. Confocal SERS and dark-field microscopy was performed at the same positions and compared to electromagnetic modeling, revealing that the enhancement factor is proportional to the number of gaps in each cluster (see Figure 6.10A).

Another factor for functional devices is the control of orientation of anisotropic nanoparticles in their self-assemblies. Figure 6.10B shows an example of a 3D self-assembled standing array of gold nanorods on micropatterned gold/glass substrates using macromolecular ligands as directing agents [79]. The anisotropic building blocks were modified with a thiol-terminated ligands consisting of oligoethylene and oligo(ethylene glycol) blocks. Upon capillary and convective assembly, vertically aligned and hexagonally close-packed multilayer colloidal crystals are formed. The interparticle gaps of 5 ± 1 nm were determined by SAXS [79] and are consistent with the proposed thickness of the ligand shell [140]. Both the high spatial ordering and the small interparticle distances increase the hot spot density, and therefore their Raman activity. The 3D nanorod arrays exhibited a 36 times enhancement compared to a commercial SERS substrate [79].

Apart from controlling the interparticle distances also the option to perform post-modification of self-assembled particle arrays opens new pathways to controlling optical properties of nanoparticles. Müller *et al*. have shown that hexagonally close-packed monolayers of gold nanoparticles can be prepared on macroscopic substrates by spin-coating of Au/PNIPAm core/shell particles [137]. In addition,

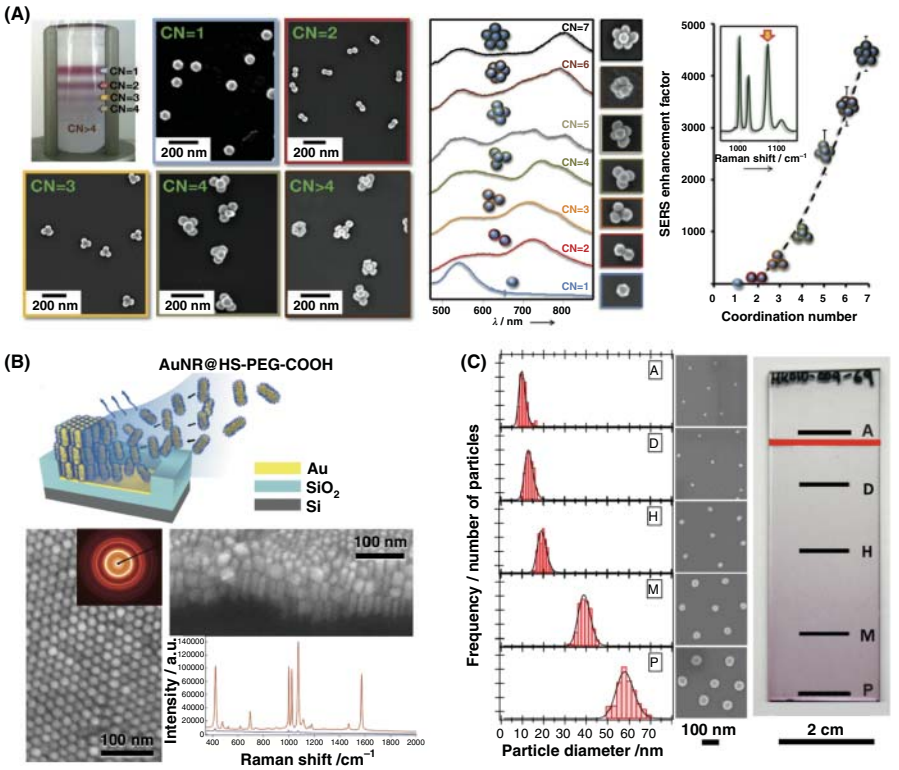

Figure 6.10 Application examples of assemblies of macromolecule-decorated nanoparticles: (A) Organized plasmonic nanoclusters assembled from gold nanoparticles with block copolymer shell. SEM images show clusters of discrete coordination numbers (CN), separated by density gradient centrifugation. Dark-field single-particle optical spectroscopy next to the corresponding clusters; SERS enhancement as a function of CNs normalize to the enhancement of a single particle. (Adapted with permission from [136]. Copyright 2012 Wiley.) (B) 3D arrays of standing gold nanorods, modified with thiol-PEO-carboxyl ligands assembled into micropatterned substrates. SEM images show top and side view of the hexagonally close packing of nanorods with interparticle gaps of 5 nm as evaluated from the transmission SAXS pattern (*see inset*). SERS enhancement was studied for benzenethiol (*see spectrum*). (Adapted with permission from [79]. Copyright 2012 Wiley.) (C) Plasmonic library based on substrate-supported gradiential plasmonic arrays with well-defined interparticle spacing: size distributions and SEM images of gold nanoparticle arrays on a macroscopic glass slide (*see photograph*). The gradual color change from nearly transparent to almost purple indicates the increasing particle sizes from top (9 nm) to bottom (57 nm) of the substrate. The monolayer assembly was achieved by spin-coating Au/PNIPAm core/shell colloids onto the substrate and subsequent overgrowth of the gold cores. (Adapted with permission from [137]. Copyright 2014 ACS.) (*See color insert for color representation of this figure*).

the authors have shown that these substrates can be used for the preparation of nanoparticle arrays with a continuous gradient in particle sizes from 9 to 57 nm (see Figure 6.10C). Consequently, this translates to a gradient in optical properties due to the size-dependent plasmonic properties of the gold particles. The gradient array was realized by immersion of a substrate-supported particle monolayer into a growing solution containing CTAB, gold ions, and a mild reducing agent (ascorbic acid). Due to the soft and porous character of the hydrogel shell of the adsorbed core/shell particles, the reactants could diffuse into the shell and allow for autocatalytic overgrowth of the gold cores. A dip-coating protocol with controlled immersion time was used to achieve a continuous gradient in particle size. Hence, the particle size became a function of the local position of the macroscopic substrate. The large separation of the gold particles, which results from the rather thick hydrogel shells, allowed avoiding aggregation and interparticle coupling of the plasmonic properties. The combination of distance control and post-modification yields a plasmonic library in form of particle arrays on macroscopic areas (see the photograph of a glass slide in Figure 6.10C) [137].

6.5 CONCLUSIONS AND OUTLOOK

This chapter gave an overview of the tools that macromolecules provide for controlling nanoparticle assemblies. At present, we can choose from a rich variety of methods for ligand exchange/coupling of both artificial and biomacromolecules. In turn, we can gain control over interparticle distances in close-packed assemblies in two and three dimensions. Linear assemblies are feasible exploiting heterogeneities in surface modification with artificial macromolecules and biomacromolecules offering access to even higher levels of complexity. Indeed structural control has already been exploited for various applications like the examples in plasmonics mentioned in the final section. Many other fields are currently emerging, such as photovoltaics [9] and biosensing [141]. Given the diversity of approaches and potential applications, it is, of course, difficult to speculate on the future of the field. Nevertheless, we want to address two remaining challenges. *Exploiting responsiveness* of macromolecular building blocks *for creating tunable nanoassemblies* is a logical next step after mastering equilibrium situations. Indeed macromolecules are or can be made sensitive to a whole range of external parameters such as solvent composition (including pH and salt concentration), temperature, and electrochemical or biochemical stimuli. Consequently the conformation/shape of nanoparticle coatings react toward those stimuli and influence the structure of nanoparticle assemblies and their structure dependent optical and electronic properties. A few works have demonstrated already the proof of concept that the responsiveness of polymer coatings can be applied to control assembly structures of nanoparticles in 2D and 3D [84, 86]. *Mechanical deformation* of the typically elastic soft polymeric coatings offers another option. While widely used for sensing and dynamic structural coloring on the scale of several hundreds of nanometers, these effects have so far been relatively little used for nanoscale distances, despite the great potential for adjusting properties. An interesting aspect

is also that the electronic/optical effects that are linked to the desired structure can be directly used as a structure guiding stimulus.

Dissipative assembly offers an exciting perspective *for adaptive materials* [86]. There are, of course, classic examples for artificial systems that illustrate the potential of shear-induced structure formation [142]. But beyond that, there are many further options for influencing structure formation by dissipative processes. Especially for biological systems, structures are usually a result of equilibrium between a structure-forming and a structure-breaking process. A typical example is the constant polymerization and depolmerization of actin [143] and other fibrillar proteins as well as the constant process of bone construction/deconstruction by osteoblasts and osteoclasts [144, 145]. This dynamic equilibrium character of biological structures is crucial for their adaptivity. Indeed supramolecular chemistry provides access to similar designs, which could lead to *living materials* that are truly adaptive and not just self-healing. Of course, biomacromolecules could as well be directly used for such approaches.

These are just some examples for the broad range of options that macromolecular design in combination with colloidal building blocks offers. Indeed, the chances are very high that the macromolecular route will develop into a cornerstone of the next generation of *materials by design*.

REFERENCES

1. Fratzl, P.; Weinkamer, R. Nature's Hierarchical Materials. *Prog Mater Sci* **2007**, *52*, 1263–1334.
2. Dunlop, J. W. C.; Fratzl, P. Biological Composites. *Annu Rev Mater Res* **2010**, *40*, 1–24.
3. Dunlop, J. W. C.; Weinkamer, R.; Fratzl, P. Artful Interfaces within Biological Materials. *Mater Today* **2011**, *14*, 70–78.
4. Lu, M.-H.; Feng, L.; Chen, Y.-F. Phononic Crystals and Acoustic Metamaterials. *Mater Today* **2009**, *12*, 34–42.
5. Liu, Y.; Zhang, X. Metamaterials: a New Frontier of Science and Technology. *Chem Soc Rev* **2011**, *40*, 2494.
6. Nicolaou, Z. G.; Motter, A. E. Mechanical Metamaterials with Negative Compressibility Transitions. *Nature Nanotech* **2012**, *11*, 608–613.
7. Lee, J.-H.; Singer, J. P.; Thomas, E. L. Micro-/Nanostructured Mechanical Metamaterials. *Adv Mater* **2012**, *24*, 4782–4810.
8. Atwater, H. A.; Polman, A. Plasmonics for Improved Photovoltaic Devices. *Nat Mater* **2010**, *9*, 205–213.
9. Karg, M.; König, T. A. F.; Retsch, M.; Stelling, C.; Reichstein, P. M.; Honold, T.; Thelakkat, M.; Fery, A. Colloidal Self-Assembly Concepts for Light Management in Photovoltaics. *Mater Today* **2015**, *18*, 185–205.
10. Zheludev, N. I.; Kivshar, Y. S. From Metamaterials to Metadevices. *Nat Mater* **2012**, *11*, 917–924.
11. Pavlidou, S.; Papaspyrides, C. D. A Review on Polymer–Layered Silicate Nanocomposites. *Prog Polym Sci* **2008**, *33*, 1119–1198.

12. Paul, D. R.; Robeson, L. M. Polymer Nanotechnology: Nanocomposites. *Polymer* **2008**, *49*, 3187–3204.

13. Möller, M. W.; Handge, U. A.; Kunz, D. A.; Lunkenbein, T.; Altstädt, V.; Breu, J. Tailoring Shear-Stiff, Mica-Like Nanoplatelets. *ACS Nano* **2010**, *4*, 717–724.

14. Bieligmeyer, M.; Taheri, S. M.; German, I.; Boisson, C.; Probst, C.; Milius, W.; Altstädt, V.; Breu, J.; Schmidt, H.-W.; D'Agosto, F.; et al. Completely Miscible Polyethylene Nanocomposites. *J Am Chem Soc* **2012**, *134*, 18157–18160.

15. Lunkenbein, T.; Kamperman, M.; Li, Z.; Bojer, C.; Drechsler, M.; Förster, S.; Wiesner, U.; Müller, A. H. E.; Breu, J. Direct Synthesis of Inverse Hexagonally Ordered Diblock Copolymer/Polyoxometalate Nanocomposite Films. *J Am Chem Soc* **2012**, *134*, 12685–12692.

16. Moffitt, M. G. Self-Assembly of Polymer Brush-Functionalized Inorganic Nanoparticles: From Hairy Balls to Smart Molecular Mimics. *J Phys Chem Lett* **2013**, *4*, 3654–3666.

17. Sarikaya, M.; Tamerler, C.; Jen, A. K. Y.; Schulten, K.; Baneyx, F. Molecular Biomimetics: Nanotechnology through Biology. *Nat Mater* **2003**, *2*, 577–585.

18. Zhang, S. Fabrication of Novel Biomaterials through Molecular Self-Assembly. *Nat Biotechnol* **2003**, *21*, 1171–1178.

19. Ahmed, T. A. E.; Dare, E. V.; Hincke, M. Fibrin: a Versatile Scaffold for Tissue Engineering Applications. *Tissue Eng, Part B* **2008**, *14*, 199–215.

20. Mattoussi, H.; Mauro, J. M.; Goldman, E. R.; Anderson, G. P.; Sundar, V. C.; Mikulec, F. V.; Bawendi, M. G. Self-Assembly of CdSe–ZnS Quantum Dot Bioconjugates Using an Engineered Recombinant Protein. *J Am Chem Soc* **2000**, *122*, 12142–12150.

21. Meyers, M. A.; Chen, P.-Y.; Lin, A. Y.-M.; Seki, Y. Biological Materials: Structure and Mechanical Properties. *Prog Mater Sci* **2008**, *53*, 1–206.

22. Minko, S. Responsive Polymer Brushes. *Journal of Macromolecular Science, Part C: Polym Rev* **2006**, *46*, 397–420.

23. Stuart, M. A. C.; Huck, W. T. S.; Genzer, J.; Müller, M.; Ober, C.; Stamm, M.; Sukhorukov, G. B.; Szleifer, I.; Tsukruk, V. V.; Urban, M.; Winnik, F.; Zauscher, S.; Luzinov, I.; Minko, S. Emerging Applications of Stimuli-Responsive Polymer Materials. *Nat Mater* **2010**, *9*, 101–113.

24. Ma, X.; Tian, H. Stimuli-Responsive Supramolecular Polymers in Aqueous Solution. *Accounts Chem Res* **2014**, *47*, 1971–1981.

25. Gil, E.; Hudson, S. Stimuli-Reponsive Polymers and Their Bioconjugates. *Prog Polym Sci* **2004**, *29*, 1173–1222.

26. Ehlert, S.; Taheri, S. M.; Pirner, D.; Drechsler, M.; Schmidt, H.-W.; Förster, S. Polymer Ligand Exchange to Control Stabilization and Compatibilization of Nanocrystals. *ACS Nano* **2014**, *8*, 6114–6122.

27. Daniel, M.-C.; Astruc, D. Gold Nanoparticles: Assembly, Supramolecular Chemistry, Quantum-Size-Related Properties, and Applications Toward Biology, Catalysis, and Nanotechnology. *Chem Rev* **2004**, *104*, 293–346.

28. Lu, A.-H.; Salabas, E. L.; Schüth, F. Magnetic Nanoparticles: Synthesis, Protection, Functionalization, and Application. *Angew Chem, Int Ed* **2007**, *46*, 1222–1244.

29. Lee, H.; Dellatore, S. M.; Miller, W. M.; Messersmith, P. B. Mussel-Inspired Surface Chemistry for Multifunctional Coatings. *Science* **2007**, *318*, 426–430.

30. Chanana, M.; Jahn, S.; Georgieva, R.; Lutz, J.-F.; Bäumler, H.; Wang, D. Fabrication of Colloidal Stable, Thermosensitive, and Biocompatible Magnetite Nanoparticles and Study of Their Reversible Agglomeration in Aqueous Milieu. *Chem Mater* **2009**, *21*, 1906–1914.
31. Sodipo, B. K.; Aziz, A. A. A Sonochemical Approach to the Direct Surface Functionalization of Superparamagnetic Iron Oxide Nanoparticles with (3-Aminopropyl)Triethoxysilane. *Beilstein J Nanotechnol* **2014**, *5*, 1472–1476.
32. Francis, R.; Joy, N.; Aparna, E. P.; Vijayan, R. Polymer Grafted Inorganic Nanoparticles, Preparation, Properties, and Applications: a Review. *Polym Rev* **2014**, *54*, 268–347.
33. Kuttner, C.; Tebbe, M.; Schlaad, H.; Burgert, I.; Fery, A. Photochemical Synthesis of Polymeric Fiber Coatings and Their Embedding in Matrix Material: Morphology and Nanomechanical Properties at the Fiber-Matrix Interface. *ACS Appl Mater Interfaces* **2012**, *4*, 3485–3492.
34. Kuttner, C.; Hanisch, A.; Schmalz, H.; Eder, M.; Schlaad, H.; Burgert, I.; Fery, A. Influence of the Polymeric Interphase Design on the Interfacial Properties of (Fiber-Reinforced) Composites. *ACS Appl Mater Interfaces* **2013**, *5*, 2469–2478.
35. Hoyle, C. E.; Bowman, C. N. Thiol-Ene Click Chemistry. *Angew Chem, Int Ed* **2010**, *49*, 1540–1573.
36. Kuttner, C.; Maier, P. C.; Kunert, C.; Schlaad, H.; Fery, A. Direct Thiol-Ene Photocoating of Polyorganosiloxane Microparticles. *Langmuir* **2013**, *29*, 16119–16126.
37. Kolb, H. C.; Finn, M. G.; Sharpless, K. B. Click Chemistry: Diverse Chemical Function From a Few Good Reactions. *Angew Chem, Int Ed* **2001**, *40*, 2004–2021.
38. Hawker, C. J. The Convergence of Synthetic Organic and Polymer Chemistries. *Science* **2005**, *309*, 1200–1205.
39. Binder, W. H.; Sachsenhofer, R. "Click" Chemistry in Polymer and Materials Science. *Macromol Rapid Comm* **2007**, *28*, 15–54.
40. Moses, J. E.; Moorhouse, A. D. The Growing Applications of Click Chemistry. *Chem Soc Rev* **2007**, *36*, 1249–1262.
41. Iha, R. K.; Wooley, K. L.; Nyström, A. M.; Burke, D. J.; Kade, M. J.; Hawker, C. J. Applications of Orthogonal "Click" Chemistries in the Synthesis of Functional Soft Materials. *Chem Rev* **2009**, *109*, 5620–5686.
42. Milner, S. T. Polymer Brushes. *Science* **1991**, *251*, 905–914.
43. Zhao, B.; Brittain, W. J. Polymer Brushes: Surface-Immobilized Macromolecules. *Prog Polym Sci* **2000**, *25*, 677–710.
44. Matyjaszewski, K.; Xia, J. Atom Transfer Radical Polymerization. *Chem Rev* **2001**, *101*, 2921–2990.
45. Choi, T.-L.; Grubbs, R. H. Controlled Living Ring-Opening-Metathesis Polymerization by a Fast-Initiating Ruthenium Catalyst. *Angew Chem, Int Ed* **2003**, *42*, 1743–1746.
46. Bielawski, C. W.; Grubbs, R. H. Living Ring-Opening Metathesis Polymerization. *Prog Polym Sci* **2007**, *32*, 1–29.
47. Hawker, C. J.; Bosman, A. W.; Harth, E. New Polymer Synthesis by Nitroxide Mediated Living Radical Polymerizations. *Chem Rev* **2001**, *101*, 3661–3688.
48. Chiefari, J.; Chong, Y. K. B.; Ercole, F.; Krstina, J.; Jeffery, J.; Le, T. P. T.; Mayadunne, R. T. A.; Meijs, G. F.; Moad, C. L.; Moad, G.; et al. Living Free-Radical Polymerization by Reversible Addition-Fragmentation Chain Transfer: the RAFT Process. *Macromolecules* **1998**, *31*, 5559–5562.

49. Braunecker, W. A.; Matyjaszewski, K. Controlled/Living Radical Polymerization: Features, Developments, and Perspectives. *Prog Polym Sci* **2007**, *32*, 93–146.
50. Tebbe, M.; Kuttner, C.; Maennel, M.; Fery, A.; Chanana, M. Colloidally Stable and Surfactant-Free Protein-Coated Gold Nanorods in Biological Media. *ACS Appl Mater Interfaces* **2015**, *7*, 5984–5991.
51. Edwards, E. W.; Chanana, M.; Wang, D.; Möhwald, H. Stimuli-Responsive Reversible Transport of Nanoparticles Across Water/Oil Interfaces. *Angew Chem, Int Ed* **2008**, *47*, 320–323.
52. Stefaniu, C.; Chanana, M.; Ahrens, H.; Wang, D.; Brezesinski, G.; Möhwald, H. Conformational Induced Behaviour of Copolymer-Capped Magnetite Nanoparticles at the Air/Water Interface. *Soft Matter* **2011**, *7*, 4267.
53. Gambinossi, F.; Chanana, M.; Mylon, S. E.; Ferri, J. K. Programming Nanoparticle Aggregation Kinetics with Poly(MeO2MA-Co-OEGMA) Copolymers. *Soft Matter* **2013**, *9*, 11046–11053.
54. Hörenz, C.; Rudolph, T.; Barthel, M. J.; Günther, U.; Schacher, F. H. Amphiphilic Polyether-Based Block Copolymers as Crosslinkable Ligands for Au-Nanoparticles. *Polym Chem* **2015**, *6*, 5633–5642.
55. Edmondson, S.; Osborne, V. L.; Huck, W. T. S. Polymer Brushes via Surface-Initiated Polymerizations. *Chem Soc Rev* **2004**, *33*, 14–22.
56. Makino, K.; Yamamoto, S.; Fujimoto, K.; Kawaguchi, H.; Ohshima, H. Surface Structure of Latex Particles Covered with Temperature-Sensitive Hydrogel Layers. *J Colloid Interf Sci* **1994**, *166*, 251–258.
57. Okubo, M.; Ahmad, H. Adsorption Behaviors of Emulsifiers and Biomolecules on Temperaturesensitive Polymer Particles. *Colloid Polym Sci* **1996**, *274*, 112–116.
58. Dingenouts, N.; Norhausen, C.; Ballauff, M. Observation of the Volume Transition in Thermosensitive Core−Shell Latex Particles by Small-Angle X-Ray Scattering. *Macromolecules* **1998**, *31*, 8912–8917.
59. Zha, L. S.; Zhang, Y.; Yang, W. L.; Fu, S. K. Monodisperse Temperature-Sensitive Microcontainers. *Adv Mater* **2002**, *14*, 1090.
60. Karg, M.; Pastoriza-Santos, I.; Liz-Marzan, L. M.; Hellweg, T. A Versatile Approach for the Preparation of Thermosensitive PNIPAM Core–Shell Microgels with Nanoparticle Cores. *Chem Phys Chem* **2006**, *7*, 2298–2301.
61. Karg, M.; Wellert, S.; Pastoriza-Santos, I.; Lapp, A.; Liz-Marzan, L. M.; Hellweg, T. Thermoresponsive Core–Shell Microgels with Silica Nanoparticle Cores: Size, Structure, and Volume Phase Transition of the Polymer Shell. *Phys Chem Chem Phys* **2008**, *10*, 6708–6716.
62. Karg, M.; Wellert, S.; Prevost, S.; Schweins, R.; Dewhurst, C.; Liz-Marzan, L. M.; Hellweg, T. Well Defined Hybrid PNIPAM Core-Shell Microgels: Size Variation of the Silica Nanoparticle Core. *Colloid Polym Sci* **2010**, *289*, 699–709.
63. Kim, D. J.; Kang, S. M.; Kong, B.; Kim, W.-J.; Paik, H.-J.; Choi, H.; Choi, I. S. Formation of Thermoresponsive Gold Nanoparticle/PNIPAAm Hybrids by Surface-Initiated, Atom Transfer Radical Polymerization in Aqueous Media. *Macromol Chem Physic* **2005**, *206*, 1941–1946.
64. Contreras-Cáceres, R.; Sánchez-Iglesias, A.; Karg, M.; Pastoriza-Santos, I.; Pérez-Juste, J.; Pacifico, J.; Hellweg, T.; Fernández-Barbero, A.; Liz-Marzan, L. M. Encapsulation and Growth of Gold Nanoparticles in Thermoresponsive Microgels. *Adv Mater* **2008**, *20*, 1666–1670.

65. Contreras-Cáceres, R.; Pacifico, J.; Pastoriza-Santos, I.; Pérez-Juste, J.; Fernández-Barbero, A.; Liz-Marzan, L. M. Au@pNIPAMThermosensitive Nanostructures: Control Over Shell Cross-Linking, Overall Dimensions, and Core Growth. *Adv Funct Mater* **2009**, *19*, 3070–3076.

66. Fernández-López, C.; Pérez-Balado, C.; Pérez-Juste, J.; Pastoriza-Santos, I.; de Lera, A. R.; Liz-Marzan, L. M. A General LbL Strategy for the Growth of pNIPAMMicrogels on Au Nanoparticles with Arbitrary Shapes. *Soft Matter* **2012**, *8*, 4165.

67. Karg, M.; Jaber, S.; Hellweg, T.; Mulvaney, P. Surface Plasmon Spectroscopy of Gold−Poly- N-Isopropylacrylamide Core−Shell Particles. *Langmuir* **2011**, *27*, 820–827.

68. Dulle, M.; Jaber, S.; Rosenfeldt, S.; Radulescu, A.; Förster, S.; Mulvaney, P.; Karg, M. Plasmonic Gold–Poly(N-Isopropylacrylamide) Core–Shell Colloids with Homogeneous Density Profiles: a Small Angle Scattering Study. *Phys Chem Chem Phys* **2015**, *17*, 1354–1367.

69. Pelton, R. Temperature-Sensitive Aqueous Microgels. *Adv Colloid Interf Sci* **2000**, *85*, 1–33.

70. Nayak, S.; Lyon, L. A. Soft Nanotechnology with Soft Nanoparticles. *Angew Chem, Int Ed* **2005**, *44*, 7686–7708.

71. Das, M.; Zhang, H.; Kumacheva, E. MICROGELS: Old Materials with New Applications. *Annu Rev Mater Res* **2006**, *36*, 117–142.

72. Hoare, T. R.; Kohane, D. S. Hydrogels in Drug Delivery: Progress and Challenges. *Polymer* **2008**, *49*, 1993–2007.

73. White, E. M.; Yatvin, J.; Grubbs, J. B., III; Bilbrey, J. A.; Locklin, J. Advances in Smart Materials: Stimuli-Responsive Hydrogel Thin Films. *J Polym Sci, Polym Phys* **2013**, *51*, 1084–1099.

74. Döring, A.; Birnbaum, W.; Kuckling, D. Responsive Hydrogels – Structurally and Dimensionally Optimized Smart Frameworks for Applications in Catalysis, Micro-System Technology and Material Science. *Chem Soc Rev* **2013**, *42*, 7391.

75. Giersig, M.; Mulvaney, P. Preparation of Ordered Colloid Monolayers by Electrophoretic Deposition. *Langmuir* **1993**, *9*, 3408–3413.

76. Ebeling, B.; Vana, P. RAFT-Polymers with Single and Multiple Trithiocarbonate Groups as Uniform Gold-Nanoparticle Coatings. *Macromolecules* **2013**, *46*, 4862–4871.

77. Vogel, N.; Fernández-López, C.; Pérez-Juste, J.; Liz-Marzan, L. M.; Landfester, K.; Weiss, C. K. Ordered Arrays of Gold Nanostructures From Interfacially Assembled Au@PNIPAM Hybrid Nanoparticles. *Langmuir* **2012**, *28*, 8985–8993.

78. Martin, J. E.; Wilcoxon, J. P.; Odinek, J.; Provencio, P. Control of the Interparticle Spacing in Gold Nanoparticle Superlattices. *J Phys Chem B* **2000**, *104*, 9475–9486.

79. Thai, T.; Zheng, Y.; Ng, S. H.; Mudie, S.; Altissimo, M.; Bach, U. Self-Assembly of Vertically Aligned Gold Nanorod Arrays on Patterned Substrates. *Angew Chem, Int Ed* **2012**, *51*, 8732–8735.

80. Nishi, H.; Kobatake, S. Facile Preparation of Gold Nanoparticle with Diarylethene Polymers by Disodium Malate and Its Photoreversible Optical Properties. *Dyes Pigm* **2012**, *92*, 847–853.

81. Simancas, K. *Entropic Death of Polyelectrolyte Brushes: Chain Stretching, Bond Scission and Surfactant Complexation*; Der AndereVerlag, **2011**.

82. Pletsch, H.; Peng, L.; Mitschang, F.; Schaper, A.; Hellwig, M.; Nette, D.; Seubert, A.; Greiner, A.; Agarwal, S. Ultrasound-Mediated Synthesis of High-Molecular Weight Polystyrene-Grafted Silver Nanoparticles by Facile Ligand Exchange Reactions in Suspension. *Small* **2013**, *10*, 201–208.
83. Jaber, S.; Karg, M.; Morfa, A.; Mulvaney, P. 2D Assembly of Gold–PNIPAM Core–Shell Nanocrystals. *Phys Chem Chem Phys* **2011**, *13*, 5576–5578.
84. Clara-Rahola, J.; Contreras-Cáceres, R.; Sierra-Martin, B.; Maldonado-Valdivia, A.; Hund, M.; Fery, A.; Hellweg, T.; Fernández-Barbero, A. Structure and Plasmon Coupling of Gold-Poly(N-Isopropylacrylamide) Core–Shell Microgel Arrays with Thermally Controlled Interparticle Gap. *Colloid Surf A* **2014**, *463*, 18–27.
85. Lu, Y.; Drechsler, M. Charge-Induced Self-Assembly of 2-Dimensional Thermosensitive Microgel Particle Patterns. *Langmuir* **2009**, *25*, 13100–13105.
86. Karg, M.; Hellweg, T.; Mulvaney, P. Self-Assembly of Tunable Nanocrystal Superlattices Using Poly-(NIPAM) Spacers. *Adv Funct Mater* **2011**, *21*, 4668–4676.
87. Tao, A. R.; Ceperley, D. P.; Sinsermsuksakul, P.; Neureuther, A. R.; Yang, P. Self-Organized Silver Nanoparticles for Three-Dimensional Plasmonic Crystals. *Nano Lett* **2008**, *8*, 4033–4038.
88. Kim, S.-H.; Lee, S. Y.; Yang, S.-M.; Yi, G.-R. Self-Assembled Colloidal Structures for Photonics. *NPG Asia Mater* **2011**, *3*, 25–33.
89. Nie, Z.; Fava, D.; Kumacheva, E.; Zou, S.; Walker, G. C.; Rubinstein, M. Self-Assembly of Metal-Polymer Analogues of Amphiphilic Triblock Copolymers. *Nat Mater* **2007**, *6*, 609–614.
90. Klinkova, A.; Thérien-Aubin, H.; Ahmed, A.; Nykypanchuk, D.; Choueiri, R. M.; Gagnon, B.; Muntyanu, A.; Gang, O.; Walker, G. C.; Kumacheva, E. Structural and Optical Properties of Self-Assembled Chains of PlasmonicNanocubes. *Nano Lett* **2014**, *14*, 6314–6321.
91. Jones, M. R.; Osberg, K. D.; Macfarlane, R. J.; Langille, M. R.; Mirkin, C. A. Templated Techniques for the Synthesis and Assembly of Plasmonic Nanostructures. *Chem Rev* **2011**, *111*, 3736–3827.
92. Watson, J. D.; Crick, F. H. C. Molecular Structure of Nucleic Acids: a Structure for Deoxyribose Nucleic Acid. *Nature* **1953**, *171*, 737–738.
93. Seeman, N. C. Nucleic Acid Junctions and Lattices. *J Theor Biol* **1982**, *99*, 237–247.
94. Mirkin, C. A.; Letsinger, R. L.; Mucic, R. C.; Storhoff, J. J. A DNA-Based Method for Rationally Assembling Nanoparticles Into Macroscopic Materials. *Nature* **1996**, *382*, 607–609.
95. Alivisatos, A. P.; Johnsson, K. P.; Peng, X.; Wilson, T. E.; Loweth, C. J.; Bruchez, M. P., Jr; Schultz, P. G. Organization of "Nanocrystal Molecules" Using DNA. *Nature* **1996**, *382*, 609–611.
96. Seeman, N. C. DNA Engineering and Its Application to Nanotechnology. *Trends Biotechnol* **1999**, *17*, 437–443.
97. Li, H.; Carter, J. D.; LaBean, T. H. Nanofabrication by DNA Self-Assembly. *Mater Today* **2009**, *12*, 24–32.
98. Condon, A. Designed DNA Molecules: Principles and Applications of Molecular Nanotechnology. *Nat Rev Genet* **2006**, *7*, 565–575.
99. Willner, I.; Willner, B. Biomolecule-Based Nanomaterials and Nanostructures. *Nano Lett* **2010**, *10*, 3805–3815.

100. Aldaye, F. A.; Palmer, A. L.; Sleiman, H. F. Assembling Materials with DNA as the Guide. *Science* **2008**, *321*, 1795–1799.

101. Choi, C. L.;Alivisatos, A. P. From Artificial Atoms to Nanocrystal Molecules: Preparation and Properties of More Complex Nanostructures. *Annu Rev Phys Chem* **2010**, *61*, 369–389.

102. Lin, C.; Liu, Y.; Yan, H. Designer DNA Nanoarchitectures. *Biochemistry* **2009**, *48*, 1663–1674.

103. Sharma, J.; Chhabra, R.; Andersen, C. S.; Gothelf, K. V.; Yan, H.; Liu, Y. Toward Reliable Gold Nanoparticle Patterning on Self-Assembled DNA Nanoscaffold. *J Am Chem Soc* **2008**, *130*, 7820–7821.

104. Wen, Y.; McLaughlin, C. K.; Lo, P. K.; Yang, H.; Sleiman, H. F. Stable Gold Nanoparticle Conjugation to Internal DNA Positions: Facile Generation of Discrete Gold Nanoparticle−DNA Assemblies. *Bioconjugate Chem* **2010**, *21*, 1413–1416.

105. Claridge, S. A.; Mastroianni, A. J.; Au, Y. B.; Liang, H. W.; Micheel, C. M.; Fréchet, J. M. J.; Alivisatos, A. P. Enzymatic Ligation Creates Discrete Multinanoparticle Building Blocks for Self-Assembly. *J Am Chem Soc* **2008**, *130*, 9598–9605.

106. Aldaye, F. A.; Sleiman, H. F. Dynamic DNA Templates for Discrete Gold Nanoparticle Assemblies: Control of Geometry, Modularity, Write/Erase and Structural Switching. *J Am Chem Soc* **2007**, *129*, 4130–4131.

107. Aldaye, F. A.; Sleiman, H. F. Sequential Self-Assembly of a DNA Hexagon as a Template for the Organization of Gold Nanoparticles. *Angew Chem, Int Ed* **2006**, *45*, 2204–2209.

108. Mastroianni, A. J.; Claridge, S. A.;Alivisatos, A. P. Pyramidal and Chiral Groupings of Gold Nanocrystals Assembled Using DNA Scaffolds. *J Am Chem Soc* **2009**, *131*, 8455–8459.

109. Fu, A.; Micheel, C. M.; Cha, J.; Chang, H.; Yang, H.; Alivisatos, A. P. Discrete Nanostructures of Quantum Dots/Au with DNA. *J Am Chem Soc* **2004**, *126*, 10832–10833.

110. Sebba, D. S.; LaBean, T. H.; Lazarides, A. A. Plasmon Coupling in Binary Metal Core–Satellite Assemblies. *Appl Phys B* **2008**, *93*, 69–78.

111. Maye, M. M.; Nykypanchuk, D.; Cuisinier, M.; van der Lelie, D.; Gang, O. Stepwise Surface Encoding for High-Throughput Assembly of Nanoclusters. *Nat Mater* **2009**, *8*, 388–391.

112. Millstone, J. E.; Georganopoulou, D. G.; Xu, X.; Wei, W.; Li, S.; Mirkin, C. A. DNA-Gold Triangular Nanoprism Conjugates. *Small* **2008**, *4*, 2176–2180.

113. Xu, L.; Kuang, H.; Xu, C.; Ma, W.; Wang, L.; Kotov, N. A. RegiospecificPlasmonic Assemblies for in Situ Raman Spectroscopy in Live Cells. *J Am Chem Soc* **2012**, *134*, 1699–1709.

114. Sebba, D. S.;Lazarides, A. A. Robust Detection of Plasmon Coupling in Core-Satellite Nanoassemblies Linked by DNA. *J Phys Chem C* **2008**, *112*, 18331–18339.

115. Sebba, D. S.; Mock, J. J.; Smith, D. R.; LaBean, T. H.; Lazarides, A. A. Reconfigurable Core−Satellite Nanoassemblies as Molecularly-Driven Plasmonic Switches. *Nano Lett* **2008**, *8*, 1803–1808.

116. Pal, S.; Sharma, J.; Yan, H.; Liu, Y. Stable Silver Nanoparticle–DNA Conjugates for Directed Self-Assembly of Core-Satellite Silver–Gold Nanoclusters. *Chem Commun* **2009**, 6059–6061.

117. Cheng, W.; Campolongo, M. J.; Cha, J. J.; Tan, S. J.; Umbach, C. C.; Muller, D. A.; Luo, D. Free-Standing Nanoparticle Superlattice Sheets Controlled by DNA. *Nat Mater* **2009**, *8*, 519–525.

118. Wang, C.; Du, Y.; Wu, Q.; Xuan, S.; Zhou, J.; Song, J.; Shao, F.; Duan, H. Stimuli-Responsive Plasmonic Core–Satellite Assemblies: I-Motif DNA Linker Enabled Intracellular pH Sensing. *Chem Commun* **2013**, *49*, 5739.
119. Nykypanchuk, D.; Maye, M. M.; van der Lelie, D.; Gang, O. DNA-Guided Crystallization of Colloidal Nanoparticles. *Nature* **2008**, *451*, 549–552.
120. Zheng, Y.; Thai, T.; Reineck, P.; Qiu, L.; Guo, Y.; Bach, U. DNA-Directed Self-Assembly of Core-Satellite Plasmonic Nanostructures: a Highly Sensitive and Reproducible Near-IR SERS Sensor. *Adv Funct Mater* **2012**, *23*, 1519–1526.
121. Schliwa, M.;Woehlke, G. Molecular Motors. *Nature* **2003**, *422*, 759–765.
122. The Lock-and-Key Principle, Volume 1, the State of the Art—100 Years on; Behr, J.-P., Ed.; 1st ed.; Wiley-VCH, **1994**.
123. Sheldon, R. A. Enzyme Immobilization: the Quest for Optimum Performance. *Adv Synth Catal* **2007**, *349*, 1289–1307.
124. Liu, W.; Wang, L.; Jiang, R. Specific Enzyme Immobilization Approaches and Their Application with Nanomaterials. *Top Catal* **2012**, *55*, 1146–1156.
125. Strozyk, M. S.; Chanana, M.; Pastoriza-Santos, I.; Pérez-Juste, J.; Liz-Marzan, L. M. Protein/Polymer-Based Dual-Responsive Gold Nanoparticles with pH-Dependent Thermal Sensitivity. *Adv Funct Mater* **2012**, *22*, 1436–1444.
126. Chanana, M.; Rivera Gil, P.; Correa-Duarte, M. A.; Liz-Marzan, L. M.; Parak, W. J. Physicochemical Properties of Protein-Coated Gold Nanoparticles in Biological Fluids and Cells Before and after Proteolytic Digestion. *Angew Chem, Int Ed* **2013**, *52*, 4179–4183.
127. Chanana, M.; Correa-Duarte, M. A.; Liz-Marzan, L. M. Insulin-Coated Gold Nanoparticles: a Plasmonic Device for Studying Metal–Protein Interactions. *Small* **2011**, *7*, 2650–2660.
128. Hanske, C.; Tebbe, M.; Kuttner, C.; Bieber, V.; Tsukruk, V. V.; Chanana, M.; König, T. A. F.; Fery, A. Strongly Coupled Plasmonic Modes on Macroscopic Areas via Template-Assisted Colloidal Self-Assembly. *Nano Lett* **2014**, *14*, 6863–6871.
129. Caswell, K. K.; Wilson, J. N.; Bunz, U. H. F.; Murphy, C. J. Preferential End-to-End Assembly of Gold Nanorods by Biotin−Streptavidin Connectors. *J Am Chem Soc* **2003**, *125*, 13914–13915.
130. Nikitin, M. P.; Zdobnova, T. A.; Lukash, S. V.; Stremovskiy, O. A.; Deyev, S. M. Protein-Assisted Self-Assembly of Multifunctional Nanoparticles. *Proc Natl Acad Sci USA* **2010**, *107*, 5827–5832.
131. Zhen, S. J.; Huang, C. Z.; Wang, J.; Li, Y. F. End-to-End Assembly of Gold Nanorods on the Basis of Aptamer−Protein Recognition. *J Phys Chem C* **2009**, *113*, 21543–21547.
132. Craig, D.; Simpson, J.; Faulds, K.; Graham, D. Formation of SERS Active Nanoparticle Assemblies via Specific Carbohydrate–Protein Interactions. *Chem Commun* **2012**, *49*, 30.
133. Höller, R. P. M.; Dulle, M.; Thomä, S.; Mayer, M.; Steiner, A. M.; Förster, S.; Fery, A.; Kuttner, C.; Chanana, M. Protein-Assisted Assembly of Modular 3D Plasmonic Raspberry-like Core/Satellite Nanoclusters:Correlation of Structure and Optical Properties. *ACS Nano* **2016**, DOI: 10.1021/acsnano.5b07533.
134. Tebbe, M.; Mayer, M.; Glatz, B. A.; Hanske, C.; Probst, P. T.; Müller, M. B.; Karg, M.; Chanana, M.; König, T.; Kuttner, C.; Fery, A. Optically Anisotropic Substrates via Wrinkle-Assisted Convective Assembly of Gold Nanorods on Macroscopic Areas. *Faraday Discuss* **2015**, *181*, 243–260.

135. Mayer, M.; Tebbe, M.; Kuttner, C.; Schnepf, M. J.; König, T. A. F.; Fery, A. Template-Assisted Colloidal Self-Assembly of Macroscopic Magnetic Metasurfaces. *Faraday Discuss* **2016**, DOI: 10.1039/C6FD00013D.

136. Pazos-Perez, N.; Wagner, C. S.; Romo-Herrera, J. M.; Liz-Marzan, L. M.; Garcia de Abajo, F. J.; Wittemann, A.; Fery, A.; Alvarez-Puebla, R. A. Organized Plasmonic Clusters with High Coordination Number and Extraordinary Enhancement in Surface-Enhanced Raman Scattering (SERS). *Angew Chem, Int Ed* **2012**, *51*, 12688–12693.

137. Müller, M. B.; Kuttner, C.; König, T. A. F.; Tsukruk, V. V.; Förster, S.; Karg, M.; Fery, A. Plasmonic Library Based on Substrate-Supported Gradiential Plasmonic Arrays. *ACS Nano* **2014**, *8*, 9410–9421.

138. Plüisch, C. S.; Wittemann, A. Shape-Tailored Polymer Colloids on the Road to Become Structural Motifs for Hierarchically Organized Materials. *Macromol Rapid Comm* **2013**, *34*, 1798–1814.

139. Alvarez-Puebla, R. A.; Liz-Marzan, L. M. SERS Detection of Small Inorganic Molecules and Ions. *Angew Chem, Int Ed* **2012**, *51*, 11214–11223.

140. Jones, M. R.; Macfarlane, R. J.; Prigodich, A. E.; Patel, P. C.; Mirkin, C. A. Nanoparticle Shape Anisotropy Dictates the Collective Behavior of Surface-Bound Ligands. *J Am Chem Soc* **2011**, *133*, 18865–18869.

141. Howes, P. D.; Chandrawati, R.; Stevens, M. M. Colloidal Nanoparticles as Advanced Biological Sensors. *Science* **2014**, *346*, 1247390–1247390.

142. Schäfer, C. G.; Winter, T.; Heidt, S.; Dietz, C.; Ding, T.; Baumberg, J. J.; Gallei, M. Smart Polymer Inverse-Opal Photonic Crystal Films by Melt-Shear Organization for Hybrid Core–Shell Architectures. *J Mater Chem C* **2015**, *3*, 2204–2214.

143. Pfaendtner, J.; La Cruz, De, E. M.; Voth, G. A. Actin Filament Remodeling by Actin Depolymerization Factor/Cofilin. *Proc Natl Acad Sci USA* **2010**, *107*, 7299–7304.

144. Clarke, B. Normal Bone Anatomy and Physiology. *Clin J Am Soc Nephrol* **2008**, *3 Suppl 3*, S131–S139.

145. Kini, U.; Nandeesh, B. N. Physiology of Bone Formation, Remodeling, and Metabolism. In *Radionuclideand Hybrid Bone Imaging*; Fogelman, I.; Gnanasegaran, G.; Wall, H. V. D., Eds.; Springer Berlin Heidelberg: Berlin, Heidelberg, **2012**; pp. 29–57.